AN IN-SITU PHOTOLUMINESCENCE STUDY OF THE EFFECT OF WET-CHEMICAL ETCHING ON SILICON QUANTUM DOTS

by

Gaute Otnes

A thesis submitted to the Faculty and the Board of Trustees of the Colorado School of Mines in partial fulfillment of the requirements for the degree of Master of Science (Materials Science).

Golden, Colorado

Date _____

Signed: _____
Gaute Otnes

Signed: _____
Dr. Reuben T. Collins
Thesis Advisor

Golden, Colorado

Date _____

Signed: _____
Dr. Thomas E. Furtak
Professor and Head
Department of Physics

ABSTRACT

Quantum dots (QDs) are semiconducting nanocrystals that are sufficiently small that size and shape can be used to control electronic properties, particularly bandgap, through the effects of quantum confinement. QDs made of silicon are gaining increasing interest due to material abundance, nontoxicity and the promise of more straight forward integration with already existing silicon technology. This gives these structures the potential to be useful in a wide range of applications, including photovoltaics, biological imaging, novel sensors, LEDs and a host of other optoelectronic technologies.

Since the properties of the QDs are size dependent, an important issue is to be able to reproducibly tune their size and to do so with a method that can be upscaled to macroscopic quantities. Further, theoretical models predict that very small Si QDs (1-2 nm) will show favorable stability and optical properties. Post growth wet-chemical etching is a promising route to size control which can also facilitate colloidal processing of the dots. A range of different etches have been thoroughly investigated for bulk silicon, but their effect on QDs is still not well understood, and reducing size into the 1-2 nm range has proven difficult. QDs of such a size would provide a system bridging the gap between theory and experiments, and open up new exciting possibilities for further discovery.

This thesis presents an investigation into size reduction by wet-chemical etching using a mixture of hydrofluoric acid and nitric acid on crystalline silicon QDs prepared by plasma enhanced chemical vapor deposition. The effects of the etch on the photoluminescence (PL) and absorption of the material are studied in-situ, which allows following the same population of dots in real time as they change size, without any material being added or lost. The PL peak can be blue-shifted over a wide wavelength range (>250 nm). However, two distinct wavelength regimes are identified where the PL emission peak cannot be changed any further. These two phenomena and their dependence on etching conditions will be discussed.

TABLE OF CONTENTS

LIST OF FIGURES

LIST OF SYMBOLS

Solar cell efficiency . . . . . η

Incoming power . . . . . P_{in}

Outgoing power . . . . . P_{out}

Open circuit voltage . . . . . V_{oc}

Short circuit current . . . . . I_{sc}

Fill factor . . . . . FF

Transition rate . . . . . $R_{i \to f}$

Initial state . . . . . $\langle \varphi_i |$

Final state . . . . . $| \varphi_f \rangle$

Density of states function . . . . . $\rho(E_f)$

Time dependent perturbation operator . . . . . H_{int}

LIST OF ABBREVIATIONS

Renewable Energy Materials Science and Engineering Center . . . . . REMRSEC

Photoluminescence . . . . . PL

Intergovernmental Panel on Climate Change . . . . . IPCC

Carbon Capture and Storage . . . . . CCS

Photovoltaic . . . . . PV

International Energy Agency . . . . . IEA

Quantum dot . . . . . QD

Highest occupied molecular orbital . . . . . HOMO

Lowest unoccupied molecular orbital . . . . . LUMO

Multiple exciton generation . . . . . MEG

Polyvinylidene fluoride . . . . . PVDF

Polymethyl methacrylate . . . . . PMMA

Porous silicon . . . . . p-Si

Plasma enhanced chemical vapor deposition . . . . . PECVD

Deionized . . . . . DI

Charge coupled device . . . . . CCD

Crystalline silicon . . . . . c-Si

Photoluminescence excitation spectroscopy . . . . . PLE

Ultraviolet-visible absorption spectroscopy . . . . . UV-VIS

Near infrared . . . . . NIR

Quantum yield . . . . . QY

Full width at half maximum . . . . . FWHM

Selected area electron diffraction pattern . . . . . SAED

Dynamic light scattering . . . . . DLS

Electron spin resonance . . . . . ESR

Time resolved photoluminescence . . . . . TRPL

Photomultiplier tube . . . . . PMT

ACKNOWLEDGMENTS

First of all I want to thank my family and my friends for all their love, support and encouragement. Without them I would have never made it through.

I would further like to express my gratitude to the U.S.-Norway Fulbright Foundation for Educational Exchange, the Johan Helmich Janson and Marcia Janson's Endowment, and the Colorado School of Mines' Office of Graduate Studies for financial support. Further I want to thank the Renewable Energy Materials Research Science and Engineering Center (REMRSEC) for access to facilities and a great research environment.

Thanks so much to my advisor, Reuben, for all his help and support in all the parts of this adventure. For his guidance and patience, and for always maintaining a humorous perspective on the ups and downs of scientific research.

A big thank you to Ingrid, for all her kind help and instruction, and for answering my endless stream of ignorant questions. She also did all the TEM imaging used in this thesis, which I am very grateful for.

Thanks to my fellow grad students for sharing this experience with me, both on and off campus. I hope and believe that the friendship we have developed will last long after our time at the School of Mines.

All the starting material that I have worked with have been grown by Chito Kendrick, Ingrid Anderson and Grant Klafehn. I thank them for their help, and apologize for nagging.

Thanks to the REMRSEC facilities manager and technicians, for maintaining the equipment I have been so dependent on, and always being ready to lend a helping hand or share a good story.

CHAPTER 1

INTRODUCTION

Solving the biggest challenges the global community faces in the 21st century will require a total reinvention of our energy system. By 2035, global energy demands are expected to grow by more than one-third, even if new policies are implemented. This is with 1.3 billion people still without access to electricity, a number expected to remain at or above one billion in 2030 [1], effectively hindering any meaningful economic development for this large fraction of the world's population. At the same time, the fourth report of the Intergovernmental Panel on Climate Change (IPCC)concluded that the climate system is warming unequivocally, with most of the warming over the past 50 years very likely due to anthropogenic emissions of greenhouse gases. A continuation of the current warming will lead to a significant change in the global climate, with potentially very negative effects for human survival such as an increase in occurrence and severity of floods and droughts, a loss of biodiversity and reduced water- and food-security. The IPCC describes these changes as *"likely to exceed the capacity of natural, managed and human systems to adapt."* [2] To stay within a safe level of warming, defined as 2 °C increase compared to pre-industrial levels, the Climate Panel projects that the global emissions of CO_2 need to be reduced by 50 to 85 % by 2050 compared to 2000. Most of these emissions are tied directly or indirectly to the energy we use, of which more than 80 % comes from fossil fuels. Both energy efficiency efforts and Carbon Capture and Storage (CCS) will need to play an important role in mitigations, but it is clear that to simultaneously combat climate change and lift billions of the world's population out of poverty, we will need a transition from a system heavily reliant on fossil fuels, to one based on renewable and sustainable sources. In this transition, solar energy will need to be an essential component.

1.1 Solar energy for the future

The energy that reaches the earth from the sun in one hour is enough to cover the global annual consumption of energy [3]. Even when you take technical limitations into account, harvesting the direct energy from the sun can provide several orders of magnitude more power than what society consumes [4]. The potential is thus enormous, and converting the sunlight to electricity directly through the photovoltaic (PV) effect or via heat, as well as to fuels via chemical routes, have attracted great attention.

1.1.1 Solar cell basics

To transform sunlight directly into electricity, two things are needed: An absorbing material where carriers, electrons and holes, are excited by the incoming light, and a way to separate the electrons and holes so they may recombine in an external circuit instead of in the material itself. The absorbing material is usually an inorganic semiconductor, where the carriers are excited across the bandgap. Organic materials can also be used as an absorber, where the carriers are excited from the highest occupied molecular orbital (HOMO) to the lowest unoccupied molecular orbital (LUMO). Separation of the excited free carriers happens either through charge-selective contacts, a built-in electric field, or a combination of the two. The selective contacts establish a concentration gradient driving the separation, while the electric field sweeps the carriers apart through a potential energy gradient. In solar cells not based on bulk inorganic semiconductors, where the absorbers' effective dielectric constant can be low, another level of complexity arises since the excited carriers are bound in excitons that need to be broken up into free carriers between the absorption and separation step. This preferably happens at an interface between two materials with a specific offset in their energy-levels, a so-called type II heterojunction[1].

One of the most important figures of merit for a solar cell is its efficiency, η, which tells how much of the optical power from the sunlight hitting the cell is converted into electrical

[1]Separation can also happen in other ways, such as at defects.

power output from the solar cell. It is given by the following equation [5]:

$$\eta = \frac{P_{out}}{P_{in}} * 100\% = \frac{V_{oc} * I_{sc} * FF}{P_{in}} * 100\% \tag{1.1}$$

where P_{out} is the power one gets out of the cell as electricity, P_{in} is the power from the light that hits it, V_{oc} is the open-circuit voltage, I_{sc} is the short circuit current, and FF is the fill factor which is ideally only a function of the V_{oc}. The open circuit voltage is dependent on the energy of the carriers being generated. Unless carriers are extracted before they thermalize (see Section 1.2.1), this energy will effectively depend on the bandgap of the material. In ideal materials higher bandgap gives higher V_{oc}. The short-circuit current on the other hand, is dependent on the number of carriers being generated, thus on the number of photons that have enough energy to excite carriers across the bandgap. From this we can understand the two main losses that we can try to minimize in an (ideal[2]) solar cell.

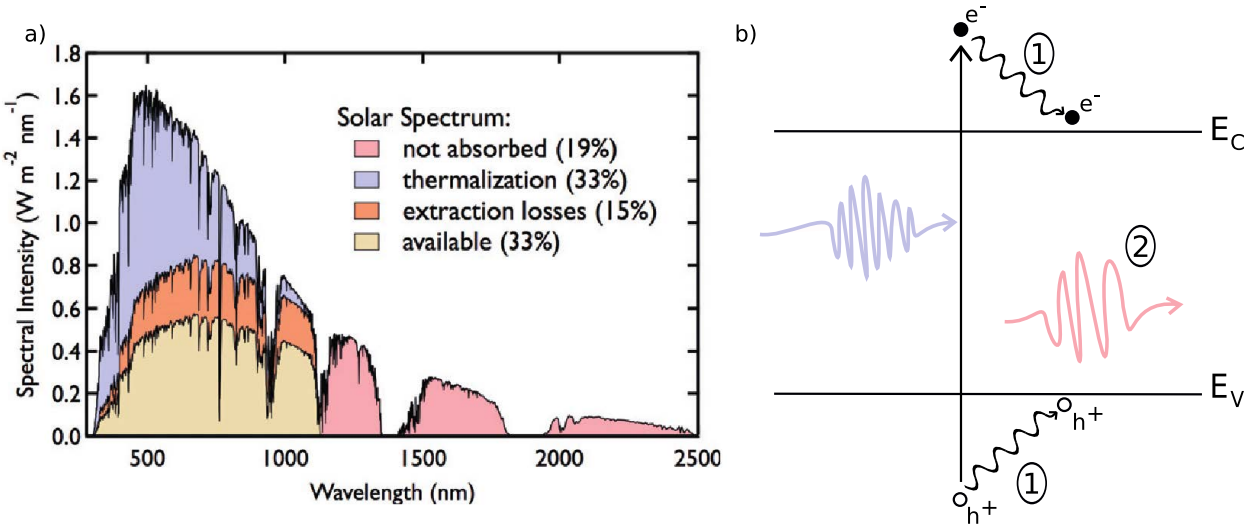

Figure 1.1: Fundamental losses in solar cells. a) The parts of the solar spectrum lost and used when accounting for minimum losses in a single-junction Si cell[7]. b) Two losses are potentially avoidable by moving to other cell-designs: 1) Thermalization losses through phonon emission, and 2) Photons not being absorbed.

[2]There are in addition many losses in a solar cell stemming from non- ideality of the cell such as resistive losses, photons lost to reflection, carriers recombining at defects etc. Such losses can affect both the V_{oc}, the I_{sc} and the FF. Much work are being put into limiting these losses in modern solar cells, such as light-trapping features and passivation of surfaces [6]. Thermodynamic extraction losses will also occur, but these are unavoidable.

These two processes, as well as the part of the solar spectrum being lost due to each of them in a single-junction silicon solar cell, are illustrated in Figure 1.1. Photons with less energy than the bandgap are lost, leading to a lower I_{sc}. Carriers receiving more energy from the photon than needed to overcome the bandgap lose this excess energy as heat when they relax to the band edge. This in turn leads to a lower V_{oc} than potentially achievable. The two mechanisms lead to a trade-off between optimizing V_{oc} or I_{sc}, and a bandgap where their product, and hence the efficiency, is maximized with regard to the solar spectrum. An analysis for a cell containing material with only one bandgap was done by Shockley and Queisser in 1961, showing that such a cell had a theoretical maximum efficiency under one sun of only a little over 30% [8], as marked in Figure 1.1 a) in beige. However, with the abundance of energy hitting the earth in the form of sunlight, even such modest efficiencies would be enough to supply all of our energy needs. Still, PV systems currently only generate 0.2 % of the global electricity generation. The reason for this lies in economy, since it is not just a question of the technology being able to produce the needed energy, but for it to do so cheaper than the competing alternatives. With these basic concepts of efficiency and economy, we can understand many of the different approaches taken within the solar cell community to compete with fossil fuels.

1.1.2 Different approaches

More than 85 % of the PV-modules in the market today are based on silicon wafers [9], which have seen a dramatic cost reduction over the recent years, largely driven by extremely low-cost manufacturing in China. However, these cells are single-junction, and are therefore limited by the Shockley-Queisser limit. It is therefore uncertain how far they can be pushed beyond the current state-of-the-art efficiency in industry of about 20 % [10][3]. The challenge is then to squeeze out the last percentages using less material and cheaper methods.

[3]The exact value is dependent on the specific technology as there are some variations, e.g. between poly- and monocrystalline silicon.

There is a wide variety of other commercially available approaches for harvesting solar energy showing potential, but they have still not gained a big share of the market. One is the multi-junction concentrator cell which bypasses the Shockley-Queisser limit by utilizing several materials with different bandgaps, hence harvesting a bigger part of the solar spectrum as efficiently as possible. These cells currently hold the world record efficiency of 44 % [11], but are still too expensive for widespread terrestrial application. In the other end of the cost vs. efficiency spectrum are the organic cells, which are currently inefficient, but hold potential for very cheap manufacturing. And finally, with more of a balance between cost and efficiency, as for conventional silicon, is a range of thin-film techniques. These can be made with substantially less material than wafer-based cells and can therefore in principle be produced inexpensively, but they have to date only a modest share of the market. Further improvement of these technologies might make significant contributions to the PV capacity.

In addition to these already commercially available technologies, a wide variety of emerging and novel approaches are being pursued where the hope is to ultimately combine very low cost and high efficiency. Such a technology would be a game-changer in the transition to a sustainable energy infrastructure. Many of the potentially transformative technologies being explored are based on utilizing, designing and controlling structures on the atomic and molecular level. One such approach is the solar cell based on quantum dots (QDs).

1.2 Quantum dot solar cells

Quantum dots are semiconductor crystals where the size of the crystal in all three dimensions is comparable to, or less than, twice the exciton Bohr radius [12]. This leads to the electrons and holes being squeezed together, effectively changing the energy levels at which they may exist. The effect can be modeled by a 3-dimensional particle-in-a-box, and solving the Schrödinger equation shows that the bandgap of the crystal will increase with decreasing size. When this effect is occurring the crystals are quantum confined, and the new and unique optical properties the material exhibits in this size-regime have attracted a lot of interest over the last decade from scientists looking to make the next generation of

solar cells.

1.2.1 Matching the solar spectrum and harvesting the hot carriers

As explained in Section 1.1.1, one of the two fundamental losses in a solar cell is photons which do not get absorbed due to insufficient energy to excite carriers across the bandgap. Harvesting more of these photons using a smaller bandgap, however, will limit the V_{oc}. Quantum dots, with their band-gaps being tunable by size, represent an opportunity to engineer a multi-bandgap cell, optimally tuned to the solar spectrum. This is similar to the multijunction cell mentioned in Section 1.1.2, but could potentially be done using only one, preferably plentiful and cheap, material, in contrast to the many rarer and very expensive elements used in the current cells utilizing such a tandem architecture.

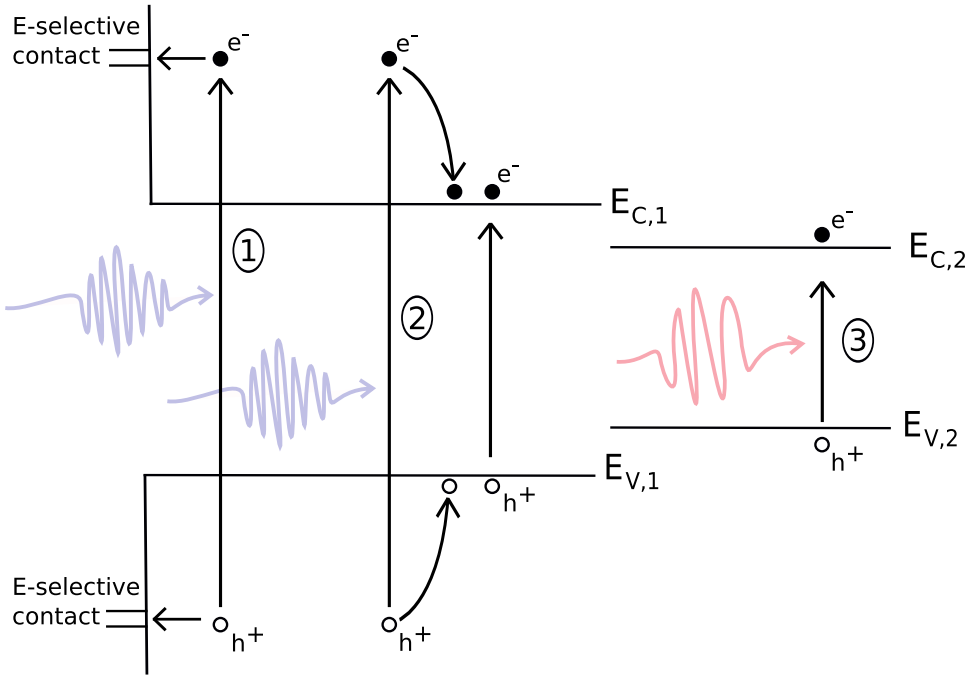

Figure 1.2: Three mechanisms through which quantum dots can boost solar cell efficiency: 1) Collecting hot carriers before they thermalize. 2) Collecting hot carrier energy through multiple exciton generation. 3) Optimally collecting photons of different energies through the use of multiple bandgaps.

The other fundamental loss involves carriers excited with more energy than the bandgap. Due to the excess kinetic energy these carriers possess they are called "hot" carriers, but

the excess energy is rapidly lost to heat, creating phonons in a thermalization process. One key to boost efficiency is therefore to try and harvest this extra energy before it gets lost, either by extracting the carrier while it is still hot, boosting the V_{oc}, or by making it generate more free carriers, boosting the I_{sc} [13]. To extract the hot electron, a process that happens faster than the thermalization is needed. One of the first suggested advantages of quantum dots, was that they would slow down the cooling of the carriers through the so-called "phonon bottleneck". As the dots enter the quantum confinement regime, the energy levels go from quasi-continuous as they are when the carriers can propagate through a periodic bulk crystal, to discretized when the boundaries of the system start to play a role. This discretization of the density of states demands multi-phonon processes to match the steps in energy. Therefore it has been proposed that the thermalization process, which occurs through phonon-emission, would slow down [13, 14]. Several reports have both supported and contradicted this phenomena, and whether it is affecting the thermalization time-scales or is being bypassed by other relaxation channels is still controversial [12]. Whether this exact phenomena is the reason or not, somewhat slowed relaxation in these systems has been observed. This has brought relaxation rates to a level (>10 ps) where the carrier extraction processes can viably compete, and this is an area of ongoing research [12].

If the excess kinetic energy of the excited carriers is bigger than the bandgap of the material, it can also use this energy to excite another pair of carriers from the valence to the conduction band (or from HOMO to LUMO) in an inverse Auger process called multiple exciton generation (MEG). This process, which is illustrated in Figure 1.2, can also happen in bulk materials, then called impact ionization, but both experimental [12, 15] and theoretical [16] work show that the process is greatly enhanced in quantum confined systems. The hope is thus to design a system where this process is so efficient, at such low energies, that it can give a meaningful boost to the solar cell efficiency.

Compared to the single junction limit of 31 %, MEG-cells have a theoretical limit of 44 %, while hot carrier cells and tandem cells (in the limit of an infinite number of bandgaps) has

an upper limit as high as 68 % under one sun [6]. However, the best laboratory quantum dot solar cells to date have only reached 7 % [17], proving that there are still significant technological challenges for these concepts to deliver on their potential. There is a broad ongoing research effort to address these issues, both with regard to cell architecture as well as choosing the right materials and giving them the proper design.

1.2.2 Why silicon?

In the study of the properties of quantum dots, and incorporation of them into prototype solar cell devices, the model systems have mainly been chalcogenide and III-V compounds such as PbSe and InP. The main reason for this is their direct bandgap, in addition to the rapid development of colloidal synthesis techniques since the beginning of the 90s, yielding high quality material with extreme size control [7]. However less successfully synthesized, characterized and utilized, quantum dots of silicon have also attracted great attention. Being earth-abundant, non-toxic, relatively inexpensive and having a rich history to borrow from in the solar cell industry, quantum dots of silicon are seen by many as a very interesting alternative to the chalcogenide and III-V dots as building blocks for the QD-solar cells. MEG have been observed in colloidal Si nanoparticles [18], and advances in both gas-phase [19] and solution synthesis [20] have sparked renewed interest in the field.

1.2.3 Are small quantum dots optimized for solar cells?

Over the last couple of years, there have been several studies suggesting that silicon QDs in the size range of 1-2 nm are of particular interest when it comes to solar cells. Ab-initio calculations predict that the MEG rate increases significantly as quantum dots get smaller [16]. Furthermore, a very important factor when incorporating QDs into solar cells is to separate the charges and transport them out of the device. This is challenging since the rules that hold for more conventional architectures do not apply. One paradigm for engineering this is to transport the charges from dot to dot bound in excitons before separation and extraction. The rate of such exciton hopping is predicted by theory to be

greatly enhanced as the dot size decreases [21]. In addition, experimental work has shown that the number of defects per dot decreases with dot size [22], which reduces any unwanted recombination. A low number of defects is also important for the dot to resist oxidation, which is a problem for Si QDs. Weighed against the presence of sharp corners between facets in very small dots (<1 nm) making them prone to oxidation, an optimized size for the dots' oxidation resistance has been predicted to exist between 1.2-2 nm [23]. Put together, these studies provide solid motivation to further study the properties of 1-2 nm sized Si QDs for application in photovoltaic devices.

1.3 Controlling the size of silicon quantum dots

Accurate size control is important not only for the production of small Si-QDs for solar cells, but also for most other applications of this material such as in QD-light emitting diodes [24], biological imaging [25] or QD-lasers [26]. However, reaching the level of size control achieved in chalcogenide and III-V quantum dots has proved challenging in silicon, both with regard to absolute size and narrow size distributions. Ideally, the size should be controlled through synthesis, however, this is currently only possible to a certain extent. Several approaches have therefore been explored to control the size through post-processing steps. Either a narrow subpopulation of a larger ensemble is selected, such as in size-selection using density gradient ultracentrifugation [27] and size exclusion column chromatography [28], or bigger quantum dots are used as starting material and then made smaller by gas-phase [29] or wet- chemical etching [30].

1.3.1 Wet-chemical etching of silicon quantum dots

Since the extensive interest in light emitting nanostructured silicon was sparked by L.T. Canham's work in 1990 [31], a variety of different wet-etching methods have been employed in top-down attempts to control the size and thereby the optical properties of Si QDs. Different mixtures of HNO_3 and HF (this etch will be further discussed in Section 2.1) have been investigated by several groups [30, 32–34]. They show that the etch is systematically blue-

shifting the photoluminescence (PL), which, according to quantum confinement, corresponds to a decreasing size, as discussed in Section 1.2, and as will be further discussed in Section 3.1. They are, however, not able to blue-shift the luminescence beyond 500 nm. Comparing with atomistic pseudopotential calculations, this corresponds to a dot size of a little more than 2 nm [35], thus right at the edge of the optimal size regime we want to explore for solar cells. The work of this thesis investigates the size control of Si QDs by applying this wet-chemical etch, and more specifically the apparent limit that exists as to how far the size can be changed.

CHAPTER 2

EXPERIMENTAL METHODS

In this chapter the general aspects of the experimental methods used in this thesis will be introduced, together with the specific setups and considerations for this study.

2.1 Wet chemical etching of silicon by a mixture of hydrofluoric and nitric acid

In processing of materials it is often useful to be able to remove matter in a controlled way. This is commonly done by etching, either dry or wet. Dry etching proceeds through bombarding the material with ions, which can remove material physically through more of a sand-blasting procedure, or chemically by free radical reactions. Wet-etching utilizes chemicals, most often acids or bases, that dissolve the material upon exposure. Depending on the application, desirable characteristics of an etch might be selectivity, isotropicity, speed, uniformity etc. These characteristics are well understood for the etches applied to silicon and its compounds [36, 37], due to its importance and long history in the microfabrication industry. One of the most common wet-etch mixtures for silicon consists of a mixture of hydrofluoric (HF) and nitric (HNO_3) acid. This mixture was thoroughly studied by Schwartz and Robbins in the years around 1960 [38–41]. They proposed a two-step mechanism where HNO_3 is oxidizing the silicon surface (Eq 2.1), followed by HF dissolving the formed oxide (Eq 2.2), effectively eating away at the silicon (Eq 2.3) [4] [42] as illustrated in Figure 2.1.

$$3Si + 4HNO_3 \rightarrow 3SiO_2 + 4NO + 2H_2O \tag{2.1}$$

$$SiO_2 + 6HF \rightarrow H_2SiF_6 + 2H_2O \tag{2.2}$$

$$3Si + 4HNO_3 + 18HF \rightarrow 3H_2SiF_6 + 4NO + 8H_2O \tag{2.3}$$

[4] The stoichiometry of this reaction is somewhat different from what was originally proposed by Schwartz and Robbins, but the overall two-step mechanism is the same.

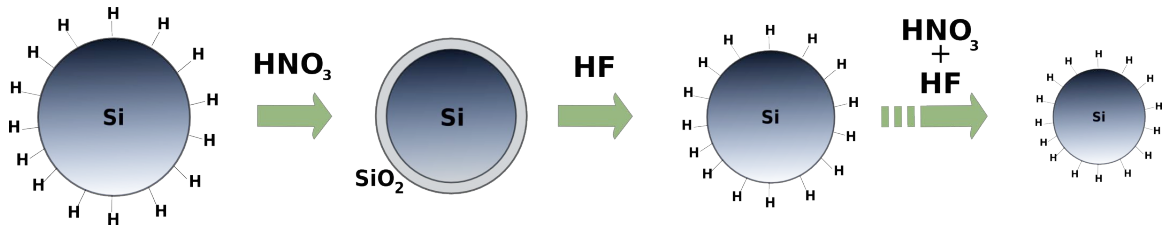

Figure 2.1: Overall etching mechanism of silicon by a mixture of nitric and hydrofluoric acid

This overall mechanism is well established, but the details of the reaction pathway, especially for the oxidizing step, is still a subject of debate. The intermediate species, the exact stoichiometry, and all the reaction products are still not finally validated, and one can find a useful summary of these points in the recent work of Acker et al [42]. Due to this ambiguity, the overall reaction is written slightly differently in different text-books and articles. Even though the exact mechanism is somewhat unclear, the effect the etch has on silicon is well characterized. It is an isotropic etch, meaning that it etches all lattice planes equally fast. The rate of the etch varies with the mixing ratio, and it is common to present the etch rates as a function of composition in a triangular plot such as the one in Figure 2.2.

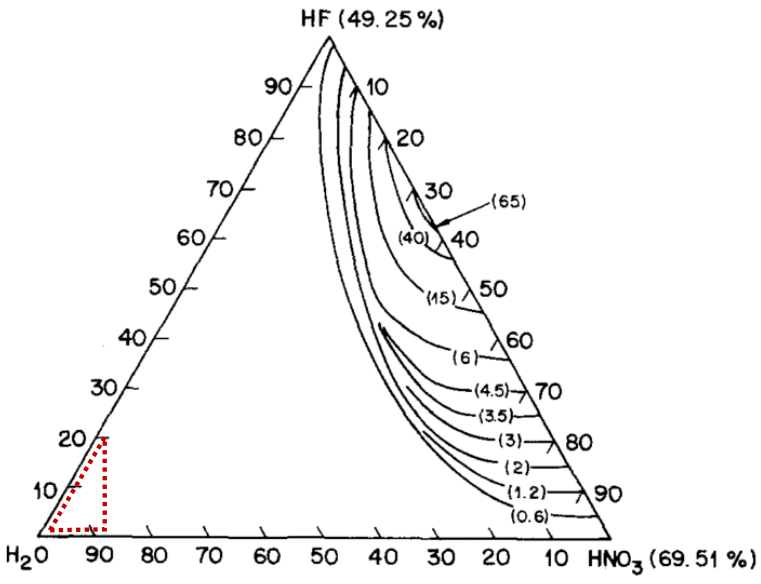

Figure 2.2: Curves of constant etch rates as a function of etchant composition for the 49% HF -70 % HNO_3 system [41]. The compositions explored in this study lies within the region indicated by the dotted red line.

It can be seen that the highest etch rate is achieved when there is a similar amount of HNO_3 and HF, while it dies off as the concentration of one of the etch-components gets low. It is established that in the HNO_3-rich regime, the etch rate is controlled by the ability of HF to diffuse to the surface. When HNO_3 is the limiting reagent however, there is still some uncertainty as to whether this is diffusion or reaction controlled, again due to the factors mentioned above [42]. In this study, the focus will be on a HNO_3-rich etch mixture in low concentrations to ensure a low etch rate, and because this is known to give a smooth and well-controlled etch [41]. The etch has a concentration of 6.8 % (v/v) HNO_3 and 0.5 % (v/v) HF unless otherwise specified. Other etch mixtures were briefly explored, all within the region indicated in Figure 2.2.

2.1.1 HF-safety

HF is a very dangerous acid, and fatal accidents from exposure of only 1 % of the total body-area have been reported for concentrated solutions, and 5 % for dilute solutions [43]. It is extremely important to ensure proper safety precautions while performing experiments involving HF. This includes acid-aprons, safety-goggles, face shield, double pair of gloves as well as long pants and closed toe shoes. The antidote to the acid, calcium gluconate, should always be readily available and clearly marked. Any exposure should be evaluated by trained medical personnel. All material, both solid and liquid, that have been in contact with HF must be collected and disposed of properly.

2.2 In-situ optical measurements

Several studies have been done on size control of nanocrystalline silicon by an HF/HNO_3-etch. The etching is normally performed for a given amount of time, and then the etch is separated from the sample by running the solution through a polyvinylidene fluoride (PVDF) membrane filter, with pore sizes of 100 nm. The nanoparticles are collected by this filter and thoroughly rinsed to remove any physisorbed acid [33]. Measurements are then performed with the dots either still on the filter, redispersed in a solvent, or after a

passivation process. Some drawbacks to this method can be identified. First, there is a question as to whether material is being lost during filtration. Second, there is a time-window between etching and measuring in which the particles might oxidize, which silicon nanoparticles very easily do. Third, only one data-point is obtained for each ensemble of dots. Therefore, ensuring that the starting material as well as the time-window and conditions between etching and measurement are identical becomes important to compare etching times or etching conditions. In this study, the optical measurements are instead performed in-situ while etching. A traditional quartz cuvette cannot be used, since HF will etch SiO_2, so instead the etching is performed in cuvettes made of plastic [5]. Such in-situ measurements while etching can potentially resolve the issues associated with the filtration, and allows to closely monitor how the properties of the same population of dots change while they sit in the etch. Similar measurements have been successfully done with porous silicon (p-Si) [44], but, to the best of my knowledge, not in freestanding Si QDs such as used here.

2.3 Growth of Si QDs by plasma enhanced chemical vapor deposition

The Si quantum dots studied in this work were all grown by plasma enhanced chemical vapor deposition (PECVD). This method of synthesizing Si-QDs was pioneered by Uwe Kortshagen and his group at the University of Minnesota [19]. A mixture of silane and argon flows through a quartz tube, with two electrodes powered by a radio-frequency power supply each looped around the tube. This creates a plasma in the gas-mixture. In this plasma the silane dissociates and Si-nanoparticles are nucleated. The particles travel with the gas flow and are collected downstream. The size and crystallinity of the particles depend on the plasma conditions, which can be changed through the processing parameters: power, gas-flow, silane concentration and chamber pressure. However, together with crystalline particles, some amorphous material is formed and this cannot be completely avoided at present. The development and exploration of this growth process has continued throughout

[5] Cuvettes made of polymethyl methacrylate (PMMA), polystyrene or a polycyclical olefin are used, depending on experiment setup and compatibility with different solvents.

the course of this work, and the starting material has therefore varied somewhat. All growths of material by PECVD have been performed by Dr. Chito Kendrick, Dr. Ingrid Anderson or Grant Klafehn.

2.3.1 Sample preparation

All experiments were performed in solutions based on deionized(DI)-water, ethanol or methanol. The starting material is Si QDs deposited on a $\sim$2.5 cm^2 piece of Si wafer by PECVD, as described in the previous section. A desired piece of the sample is selected by simply cleaving the wafer. The Si QDs come off the wafer and are dispersed in the wanted amount of solvent by five minutes of light sonication. This creates a homogeneous and somewhat cloudy suspension with a faint yellow color. These dots are then transferred to a cuvette for optical measurements. Etchant is added directly to this cuvette at the beginning of the etch experiment.

2.4 Photoluminescence spectroscopy

Photoluminescence is an important technique for studying the optical properties of semiconductors. Light emission, or luminescence, from a sample comes from the radiative recombination of an electron and a hole. In photoluminescence these are created by the absorption of a photon, in contrast to electroluminescence where the e-h-pairs are created by injection of charge. Absorption of the incoming photon might happen if it has enough energy to promote the carriers from their equilibrium state to an allowed excited state. In a semiconductor this normally means an energy higher than the bandgap. What is measured in a PL measurement is the number of photons as a function of wavelength emitted as the excited carriers find their way back to their equilibrium configuration. In the simplest scenario, only two states would be involved in the transition. The energy would then be the energy difference between the excited and the equilibrium state, while the number would be equal to the number of photons absorbed. However, there is always non-radiative transitions contributing to parts or all of this relaxation, and there might be several states from which radiative recombi-

nation can occur. PL can be used to probe these radiative recombination processes in a material, both with regard to the energy levels involved and the relative contribution from the different processes. This will be decided by the probability of the different transitions, which quantum mechanically is described by Fermi's Golden Rule, given in Equation 2.4 [45].

$$R_{i\to f} = \frac{2\pi}{\hbar}|\langle\varphi_i|H_{int}|\varphi_f\rangle|^2\rho(E_f) \tag{2.4}$$

Here $R_{i\to f}$ is the transition rate, meaning the probability per unit time for a transition of a carrier from the initial state $\langle\varphi_i|$ to the final state $|\varphi_f\rangle$, which are eigenstates of the unperturbed Hamiltonian, i.e. the Hamiltonian for the system in equilibrium. More states for the carrier to transition into will give a higher probability of transition, therefore the degeneracy of $|\varphi_f\rangle$-states must be accounted for by multiplying with the density of states function $\rho(E_f)$. H_{int} is an operator representing the time-dependent perturbation of the system. The perturbation is what is coupling the initial to the final state, in our case an interaction with the electromagnetic field through a photon[6]. $\langle\varphi_i|H_{int}|\varphi_f\rangle$ is called an overlap integral and tells how well the photon couples the initial and final state. In this context, a language where transitions are characterized as "strong" or "weak" is commonly used, and it is often referred to a transition's oscillator strength. The oscillator strength is, as the transition rate in Equation 2.4, proportional to the square modulus of the overlap integral for the transition. It is simply a measure of how likely it is for a transition to happen through absorbing or emitting a photon. Through this mathematical framework, all the possible transitions in a system can potentially be accounted for, both for absorption and emission as well as inter- and intra-band transitions. The transitions with the fastest rates will dominate the emission.

[6]It is worth noting that H_{int} will be different for emission happening in the presence of a photon, so-called stimulated emission, and for spontaneous emission.

2.4.1 Photoluminescence experiment setup

The photoluminescence setup mainly used in this study is custom made[7], built under the supervision of Professor Reuben T.Collins. It has the flexibility of having multiple excitation sources, both with a mercury-arc lamp and an argon-ion laser. Another benefit is the detection system. The luminescence is focused into a spectrometer, where a diffraction grating separates the different wavelengths spatially onto a crystalline silicon (c-Si) charge-coupled device (CCD)-array. This allows for parallel detection of spectra, which is very useful for in-situ measurements where the photoluminescence changes over time. The CCD-array is cooled using liquid nitrogen to a set temperature of -120 °C, to reduce thermal noise.

For all PL experiments, unless otherwise stated, the excitation wavelength is 365 nm, with a power of ∼1.5 mW and a beam size of ∼10 mm^2, giving an approximate power density of 15 mW/cm^2. The sample is mixed with the etchant in a cuvette, and placed so that the center of the cuvette is aligned with the slit of the spectrometer. The cuvette sits on a stirplate with a stirbar inside continuously stirring to ensure uniform etching. It is held in place by a custom made wooden holder. A sketch of the setup is shown in Figure 2.3. The software is set up to acquire spectra at given time intervals, thus following the development of the PL in time.

2.4.2 Subtraction of background signal and correction for spectral response

A problem with the plastic cuvettes used to allow for etching in-situ is that they emit light under UV-radiation. A photoluminescence spectrum of an empty PMMA cuvette is shown in Figure 2.4 a) as an example, cut off on the high-energy side by a 400 nm longpass filter. This background signal needs to be subtracted off the measured signal to reveal what is truly coming from the sample. Unfortunately, the intensity of the cuvette-luminescence is not stable throughout a measurement. This is attributed to the presence of scatterers in the sample, as well as variation in the amount of light that is absorbed by the QDs. However,

[7]Specifications of the setup and the components can be found in Appendix A

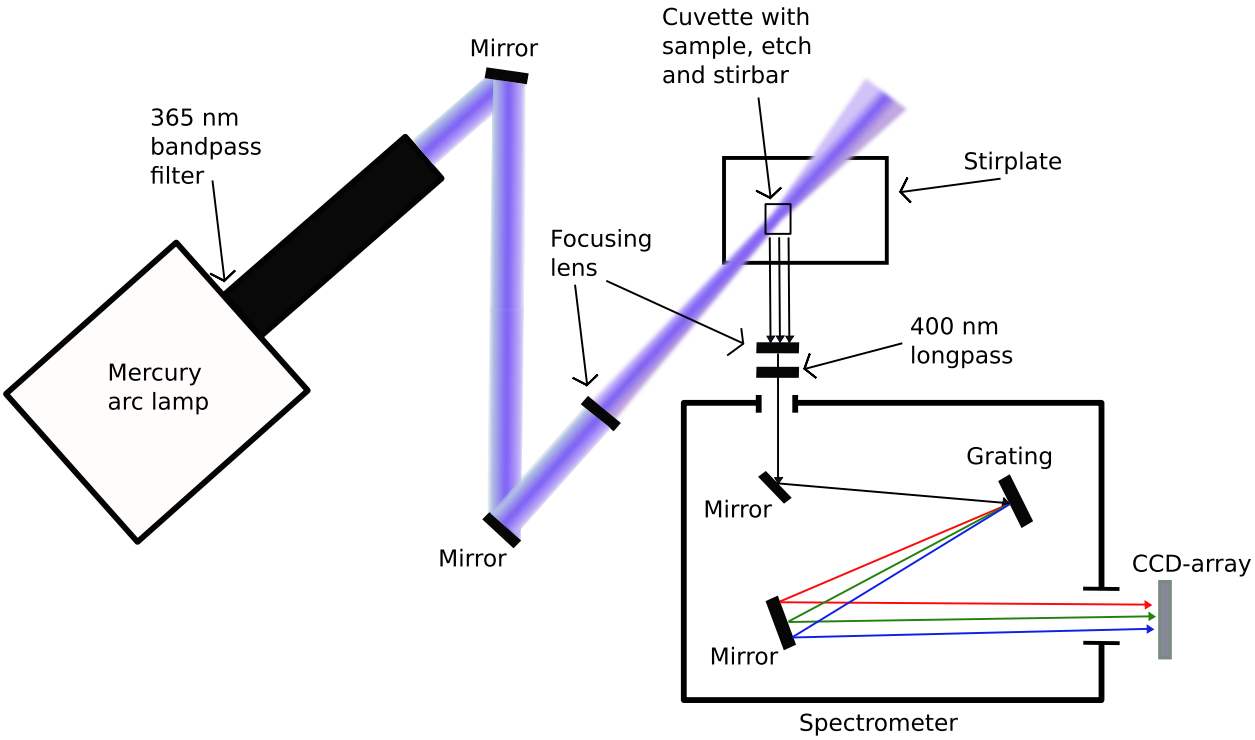

Figure 2.3: Schematic illustration of the in-situ PL setup. The sample is etched while being excited by 365 nm light from a mercury-arc lamp. The detection setup consists of a spectrometer coupled to a c-Si CCD-array.

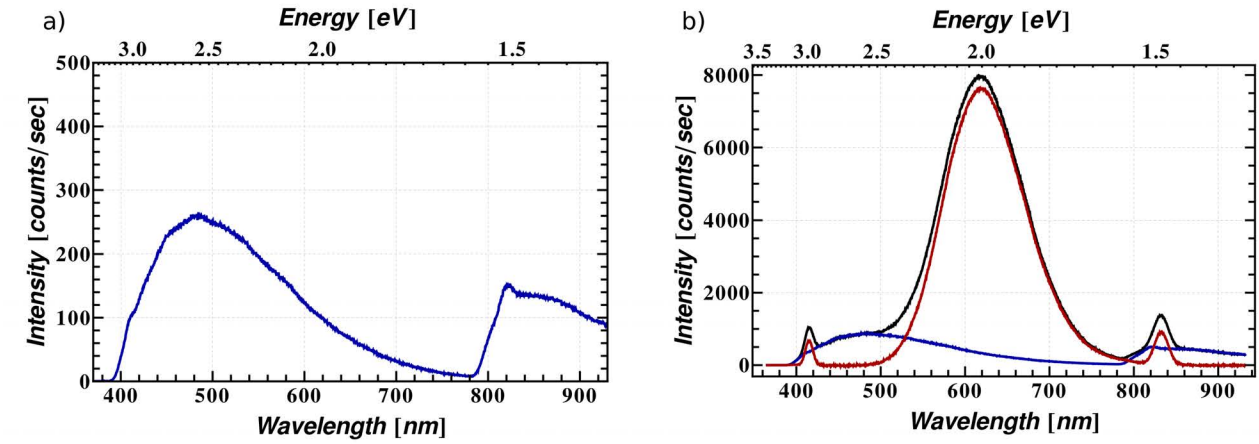

Figure 2.4: Subtracting background signal from cuvette. a) Luminescence signal from PMMA cuvettes when illuminated with 365 nm light. b) Cuvette background signal (blue) is scaled to measured signal (black) at 420 nm and subtracted off, yielding PL-signal from the sample (red). The sharp peak at 415 (and at 830 nm in 2nd order) will be discussed in Section 2.5.2

all tests indicate that the shape of its luminescence signal is not changing. Therefore, the background signal is scaled to the measured signal at 420 nm, where there is no or minimal contribution from the sample, and this scaled background signal is subtracted off. An example of a measured spectra, the scaled background signal and the resulting signal from the sample is shown in Figure 2.4b).

The detection part of the photoluminescence setup, consisting of the spectrometer and the CCD-array, are not equally efficient detecting light at all energies. A spectral response correction was applied to all spectra presented in this study. Further detail on the correction factors and how they were obtained can be found in Appendix A.1.1

2.5 Photoluminescence excitation spectroscopy

Photoluminescence excitation spectroscopy (PLE) is a special type of absorption spectroscopy. A detector is set up to measure the emission from the sample, with a monochromator allowing only light from a narrow spectral window to reach the detector. The excitation wavelength is then scanned through the spectral region of interest, and the intensity of the emission is recorded as the excitation energy changes. In contrast to ultraviolet-visible absorption spectroscopy (UV-VIS), where everything which is absorbing in the sample is measured, PLE only measures the absorption contributing to PL emission at a certain wavelength. Separation of absorption from luminescing material versus non-luminescing material such as matrices, solvents or "dark" dots is therefore possible, as well as probing a subset of nanocrystals emitting at a particular energy. Assuming that surface chemistry and shape is similar throughout the ensemble, probing of the absorption of a narrow subset of dot sizes is thus possible.

2.5.1 Photoluminescence excitation experiment setup

For PLE experiments, the setup used is a turnkey NanoLog system from Horiba Jobin Yvon[8]. The sample is placed in the cuvette holder on the sample stage, and PL and PLE

[8]Full system specifications can be found in A.1

spectra are acquired alternately in two minute intervals. Thus, a PLE spectrum is acquired every four minutes, as is a PL spectrum, and they are offset by two minutes. Between each measurement, the cuvette is taken out and stirred for about 30 seconds, to ensure uniform etching. The emission detection wavelength in the excitation scan is chosen based on the peak wavelength of the previous emission spectra.

2.5.2 Raman scattering from the solvent

When doing PLE scans, two narrow peaks often show up in the low-energy end of the spectrum. These are especially pronounced when the signal from the sample is low. A comparison with the literature show that the two peaks have an energy difference from the emission detection wavelength that perfectly match up with the OH- bending and OH-stretching modes in water [46]. Thus, the peaks originate from Raman scattering, which happens when a photon is inelastically scattered by a molecule. The photon loses some of its energy to the molecule by exciting vibrational modes, in this case bending and stretching of the OH-groups. An alternative solvent with smaller scattering cross-section or non-conflicting modes, that are in addition compatible with the etch mixture is not obvious. The simplest solution is therefore to use as high sample concentration as possible, to make the peaks less pronounced compared to the sample-signal. When mixing ethanol in the etching solution, Raman peaks corresponding to modes in the methyl group show up in the spectrum. A Raman shift of the 365 excitation source in the PL experiments are also observed, as shown in Figure 2.4 b) at 415 nm (and in second order at 830 nm). This is due to OH-stretching, as the OH-bending peak is here removed by the longpass filter placed in front of the detector to remove the excitation beam. However, in the PL experiments the peaks are not in a range where low signal from the sample needs to be detected, and have therefore not interfered notably with the results.

2.6 Transmission electron microscopy

The resolution of any imaging technique where waves are used is limited by their wavelength. Electrons accelerated to high energies can achieve much shorter wavelengths than visible light. Hence, electron microscopes are superior to optical ones when it comes to imaging on the nanometer scale. In a transmission electron microscope (TEM), a high energy electron beam is transmitted through a thin sample. Electrons can interact with both the electron clouds and the nucleii in the sample, and give rise to a range of different signals. These can all be acquired and together they can provide a wide range of different information about the specimen.

All TEM imaging in this study was performed by Dr. Ingrid Anderson.

CHAPTER 3
EXPERIMENTAL RESULTS

The main technique of this study is PL-spectroscopy, introduced in Chapter 2. Its use in understanding the behavior of Si QDs will now be discussed. Thereafter, results of the in-situ etch study will be presented.

3.1 Introduction to photoluminescence from Si QDs

Silicon is an indirect bandgap material meaning that the energy-maximum of the valence band and the energy-minimum of the conduction band are not at the same point in k-space, but at Γ and Δ respectively. Consequently, a bandedge-to-bandedge transition must involve a phonon to provide simultaneous conservation of energy and momentum. This leads to a small oscillator strength for the transition and silicon is hence a poor light emitter. Therefore it caused great excitement when L.T. Canham reported on bright red luminescence from nanostructured silicon in 1990 [31]. Luminescence from different varieties of Si nanoparticles and other nanostructures has been investigated heavily ever since, but pinning down the exact nature and origin of the light emission has proved arduous.

The luminescence typically has a broad Gaussian shape attributed to inhomogeneous broadening effects such as the size distribution of the particles and phonon assisted transitions [47, 48]. This broad peak can be changed from the near infrared (NIR) and well into the visible spectrum. Many groups have shown that the luminescence energy correlates well with size, which support the luminescence originating from quantum confined exciton recombination [34, 48–53]. Within this explanation the strongly enhanced photoluminescence is explained by quantum size effects. Many refer to the relaxation of momentum conservation, which can be understood in terms of Heisenberg's uncertainty principle. This states that increased certainty in size due to confinement will lead to a greater uncertainty in momentum. As the uncertainty of the momentum becomes comparable to or bigger than the change in

momentum needed for the $\Gamma \rightarrow \Delta$ transition, the requirement of momentum conservation will loosen. The bandgap becomes what is termed pseudo-direct. However, there is a second competing class of explanations as to what is causing the luminescence, emphasizing the role of surface states [54]. This is supported by the PL peak wavelength changing with chemical environment [55, 56], apparent inconsistency between size and PL [57], and the PL peak having an insensitivity to a high magnetic field [58]. A high magnetic field should lead to greater localization for a quantum confined exciton, but not for an already highly localized defect state. However, it is becoming increasingly clear that none of these models can fully explain all luminescent properties of Si QDs. Different mechanisms can dominate in different systems, or even both be present within the same material [54, 55, 58].

3.2 Etching can blue-shift luminescence over a wide wavelength range

Many groups have shown that applying a HF/HNO_3 etch to Si QDs or p-Si gives a blue-shift of the photoluminescence peak, and that the blue-shift increases with etch time [30, 32–34, 59]. Results of several studies, looking at both HF-rich and HNO_3-rich etching mixtures, are summarized in Figure 3.1.

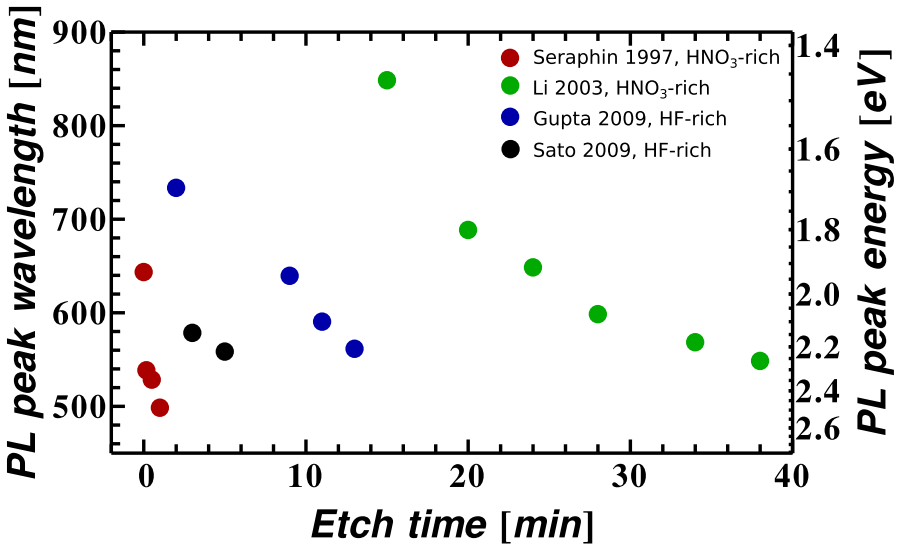

Figure 3.1: PL peak wavelength vs etch time for a number of published studies on SiQDs and p-Si [30, 32–34]

This etching process was studied using the setup for in-situ measurements described in Section 2.4.1. A series of spectra is shown in Figure 3.2, where the color of the curves change from red towards blue with increasing etch time. The peaks were fitted to a Gaussian function using Wolfram Mathematica [60]. PL peak emission wavelength and intensity from these fits are plotted as a function of etch time in Figure 3.3. Several interesting things can be noted in the time-evolution of the PL peak. Both the change in peak emission wavelength and

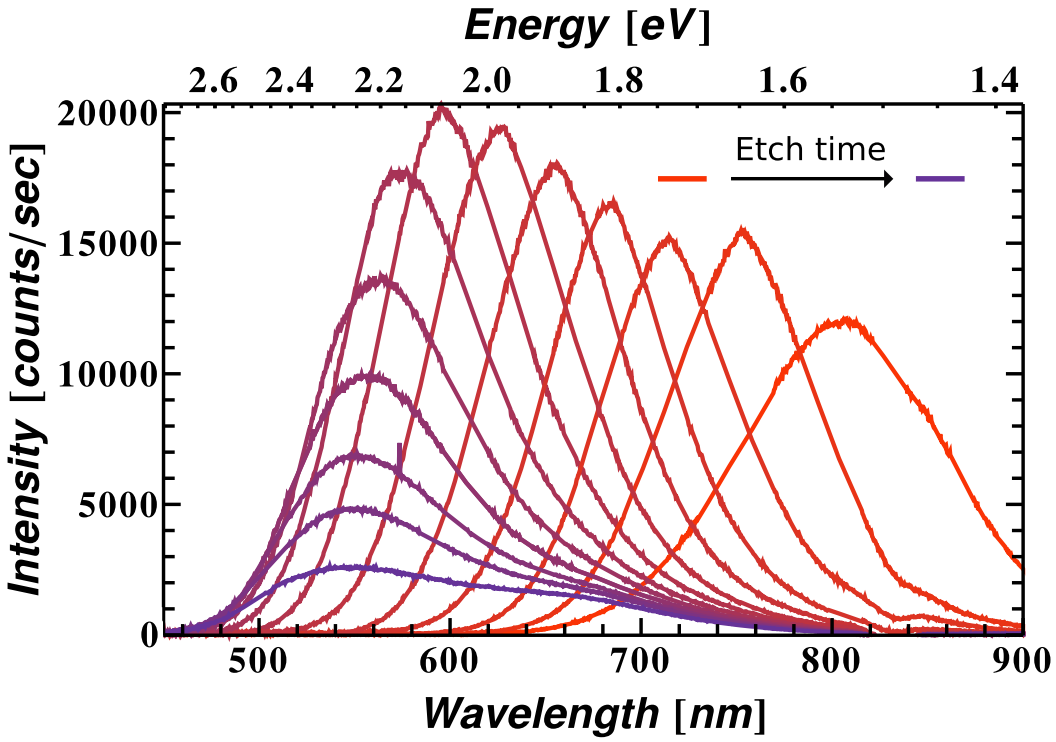

Figure 3.2: Time evolution of PL spectra during in-situ etching. Color of the curve changes from red to blue with increasing etch time.

intensity indicate that the first minute, i.e. the first two data points, work as an incubation time for the etch[9]. After that, the peak emission wavelength changes steadily (Figure 3.3 a)) over a range of almost 250 nm. Such a blue-shift as the etch proceeds indicate that the PL emission is due to the recombination of quantum confined carriers. Theoretically, many different approaches have been used to predict the relationship between the size of Si QDs and the optical gap [35, 61–63]. One is atomic pseudopotential calculations, which indicate

[9]Such an "incubation time" has been observed several times, but is not the norm in these experiments.

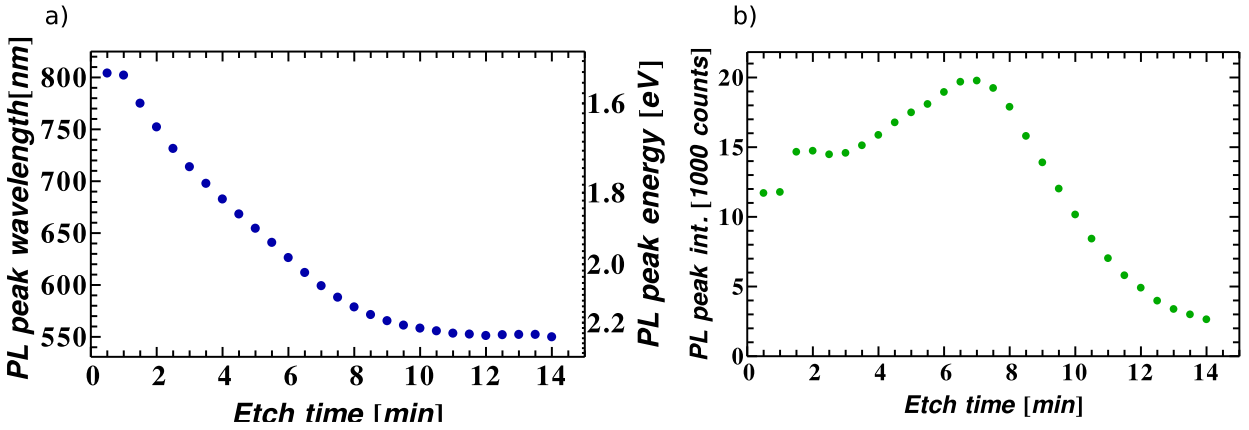

Figure 3.3: Change in PL peak emission wavelength and intensity with etch time. a) Time-evolution of peak emission wavelength. b) Time evolution of peak intensity.

that the observed blue-shift in wavelength corresponds to a change in mean size from ∼4 nm to ∼2.2 nm [35]. During this size change, there is a trend toward increasing PL intensity. This begins with an abrupt change seen during the first minute. Since the PL emission wavelength do not change during this time, it is reasonable to assume that this behavior is connected to oxide on the surface being etched away and dangling bonds being passivated. After that, the change is smooth, with the peak wavelength decreasing by almost 100 nm at fairly constant intensity. Thereafter, the intensity increases as the peak emission wavelength is shifted further, from 700 to 600 nm. Theoretical studies have been presented indicating that due to quantum confinement, the oscillator strength of the band to band transition increases exponentially with decreasing size [35, 64]. Hence, the PL emission enhancement seen here is again consistent with quantum confinement related PL. It is also seen that the peak is narrow and well defined throughout the etch, indicating a tight size distribution. In summary, the observed blue-shifting of the PL emission wavelength from 810 nm down to about 600 nm is fully consistent with a model where the decrease in dot size increases the bandgap due to quantum confinement. This indicates that the application of an etch mixture of HF and HNO_3 can indeed make the Si QDs smaller. And even more interesting, the effect of the size change on the optical properties can be followed in real time, in the same population of dots.

When the peak reaches 600 nm, the rate of blue-shifting decreases and the peak emission wavelength stabilizes at about 550 nm (2.25 eV). Being pinned at this wavelength, the luminescence intensity steadily decreases and dies away[10]. The point where the peak wavelength shifting slows down coincides with the maximum peak intensity, which is easily seen in Figure 3.2. This behavior sheds light on the studies summarized in Figure 3.1. All other groups (with a small exception of Seraphin et al.) have very similar end- points for their etch studies, where they were not able to go to higher energies[11]. Since a very similar limit is observed in the in-situ experiment, where no material is lost during filtration, one can conclude that this seems to be an inherent effect of the etching process. Even though this phenomena has been observed in many studies, no conclusive explanation has yet been put forward. It has been speculated that the etch is self-limiting, with the etch being unable to dissolve the silicon when the dots reach a certain size [44, 59]. If this is the case, the results of the present study suggest that there also exists a mechanism through which the photoluminescence is being quenched. This pinning behavior will be further discussed in Section 3.2.6, in light of results that will be presented below.

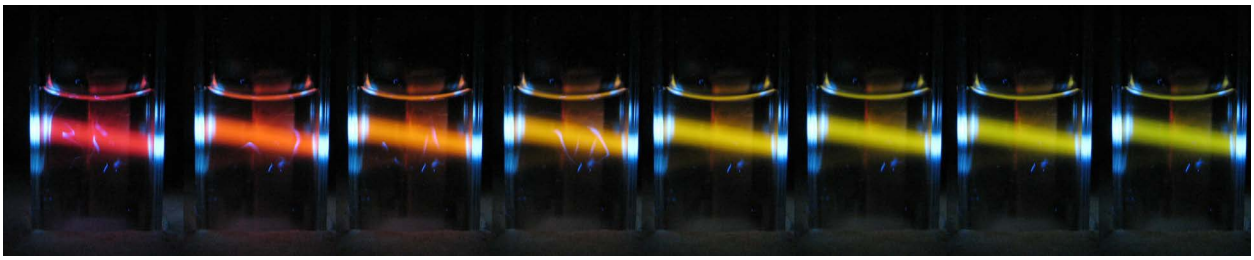

Figure 3.4: Change of luminescence color during etching. Images were taken during in-situ etching over a period of 15 minutes. The luminescing region is defined by the excitation beam passing through solution.

[10]It should be pointed out that the exact wavelength where the peak disappear has some uncertainty to it. This is simply because the wavelength where the luminescence vanishes coincides with where the background signal from the cuvette starts to get stronger (see Figure 2.4). Consequently, separating the sample signal from the background in a reliable way is hard at this stage of the etch. However, the general wavelength range where this happens is unambiguous.

[11]A similar short wavelength limit seems to have been observed in other studies as well, even though they do not include detailed data on PL-peak vs etch time [25, 65–68].

The blue-shifting of the luminescence as the dots are etched is also clearly visible to the naked eye, as illustrated in Figure 3.4.

3.2.1 Illumination dependent etch rate

Etching the silicon proceeds through a redox-reaction, thus an exchange of electrons between atoms. UV-light efficiently excites electrons in the sample, and is therefore likely to affect the etching reaction. This effect was probed in an experiment where the sample was etched in the same in-situ setup as earlier (see Section 2.4.1). It was alternated between letting the sample etch in total darkness, with the beam blocked between measurements, and under constant illumination. When the beam was blocked between measurements the sample was illuminated for about 10 seconds every minute to acquire the spectrum. The resulting change of PL peak emission wavelength is summarized in Figure 3.5. It is seen

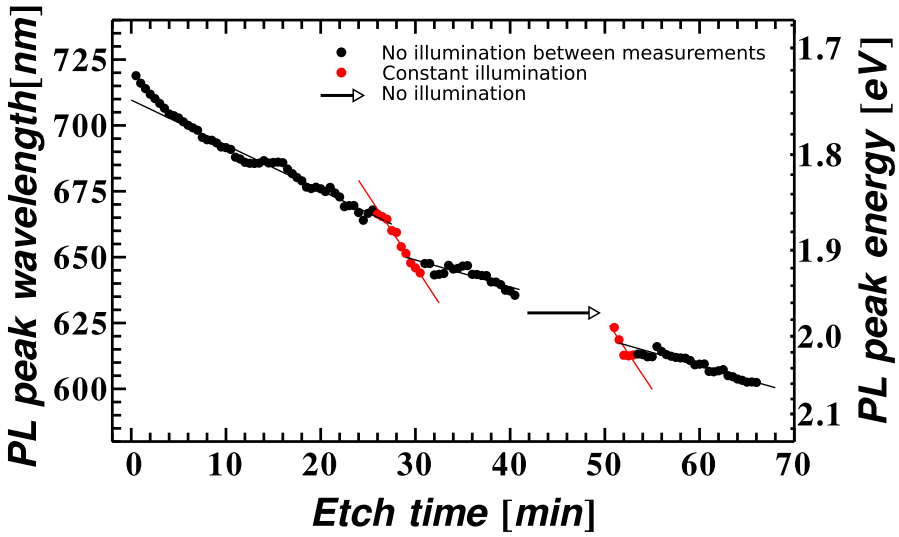

Figure 3.5: Effect of illumination on etch rate. Black data-points represents the sample being etched in the dark, only illuminated for about 10 seconds every minute to do the measurements. The red data-points represents etching under constant illumination. The break with no data-points represents etching in total darkness.

that the UV-illumination is significantly speeding up the etch. Comparing the linear fits of the black and the red data-points and adjusting for the different illumination times, the etch

rate is increased by about an order of magnitude from no illumination to full illumination. This is consistent with studies done in porous silicon [44, 69], as well as in nanocrystals of germanium [70]. Also, greatly enhanced oxidation under UV-illumination has been observed in bulk silicon [71, 72]. Thus, a reasonable explanation for the increased etch rate is that the UV illumination is enhancing the oxidation step (Equation 2.1) of the etch. However, the Veinot-group in Alberta has shown that illumination can drive the etching of silicon without oxidizing species in the etch solution. They explain this by the etch proceeding through an exciton mediated pathway. Here, the attack of silicon by HF is allowed by polarization of the Si-H bond by a photo- excited hole localized at the surface, instead of by the formation of a polar Si-O bond through oxidation [73]. It is possible that both of these mechanisms play a role in the observed effect on the etch rate.

3.2.2 PL-wavelength gets pinned- different regimes

All experiments show a shifting of the PL peak in the beginning and a stable PL peak wavelength towards the end, with decreasing intensity at the stable end-wavelength. Two

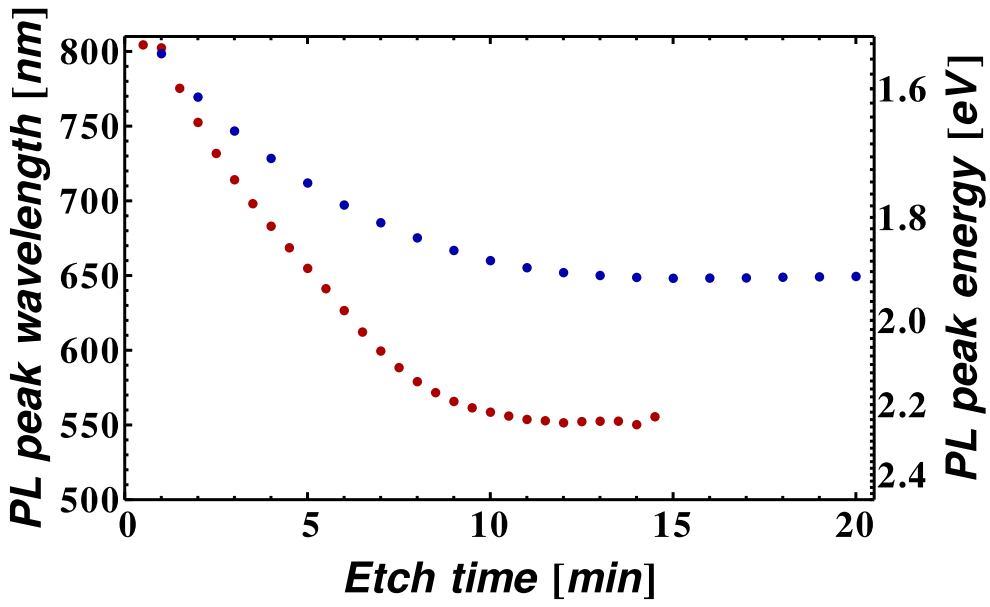

Figure 3.6: Two distinct pinning regimes for the PL peak wavelength are observed, one at 520-560 nm, and one at 620-680 nm.

distinct regimes for where the PL peak stabilizes are observed. In some of the experiments the peak goes down to 520-560 nm before it gets pinned and goes away, as discussed in Section 3.2. Another group of experiments show the peak stabilizing between 620 and 680 nm, most often very close to 650 nm. These two behaviors will from now on be referred to as the "550-regime" and the "650-regime", respectively. An example of two such experiments is shown in Figure 3.6.

If all luminescence is due to quantum confined exciton recombination, the two pinning regimes would point to the etch being self-limiting at two different sizes. However, the two pinning wavelengths are sometimes observed simultaneously in the same sample. Figure 3.7 a) shows a peak that has been shifted down from 750 nm to about 570 nm. When

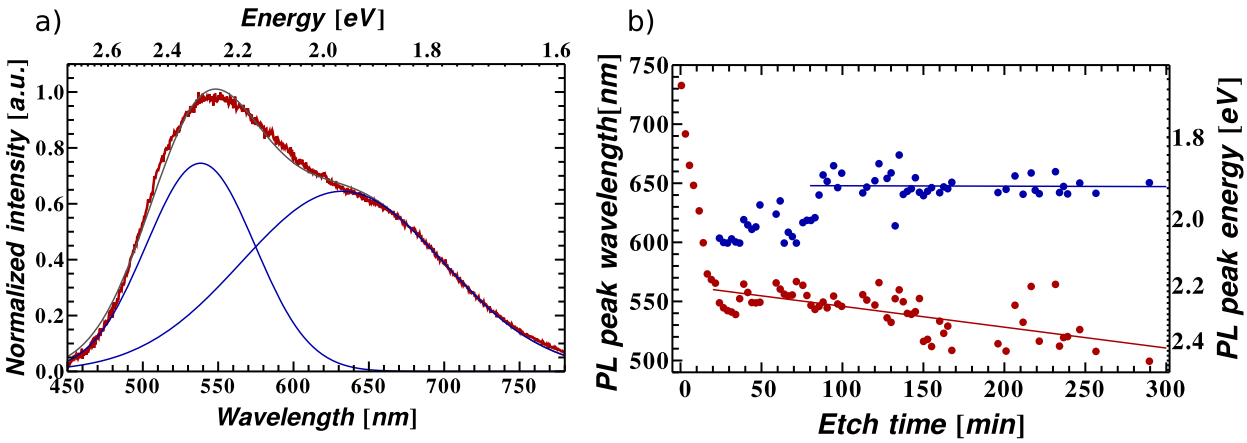

Figure 3.7: A double peak structure in the PL-signal. a) In a sample where the PL peak wavelength has been blue-shifted to the 550-regime and died off in intensity, a second lower energy peak becomes visible. The double peak can be deconvoluted using a sum of two Gaussian functions. b) Plot of deconvoluted peak emission wavelengths vs. etch time.

the shifting of the peak slows down and the intensity starts to decrease, it is seen that a second peak is present in the luminescence spectrum, which was not visible in the beginning. A deconvolution of the double peak structure is done by applying the NonLinearModelFit feature of Wolfram Mathematica using a sum of two Gaussian functions. The resulting peak wavelengths are plotted against etch time in Figure 3.7 b). Clear trends can be identified, despite considerable noise. While the low energy peak stabilizes in the 650-regime, the high

energy peak shifts slowly into the 550-regime. Thus luminescence corresponding to both of the two pinning regimes are observed in the same sample. While the peak in the 550-regime vanishes, the peak at 650 nm does decrease in intensity, but does not go away completely. This holds even when more etchant is added, as well as when the sample is left in the etch over night. The reason for this is found to be material that is not staying in solution. While no indications of such material were seen through normal visual inspection of the cuvette, the luminescence from the material makes it easily detectable under UV-illumination in a dark room. Bright luminescence is both seen from dots clinging to the walls, floating on the surface and fallen to the bottom of the cuvette.

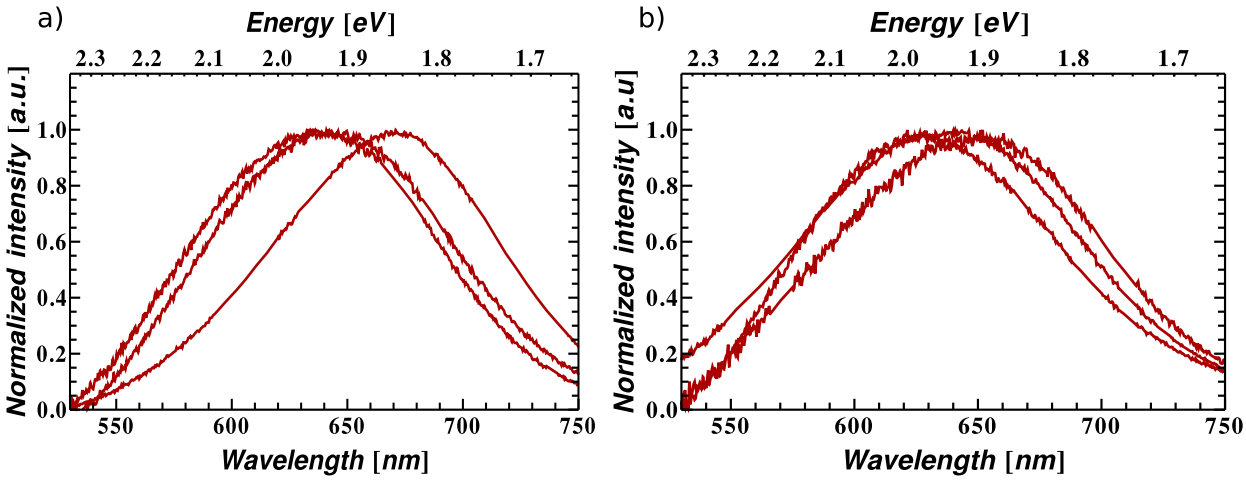

Figure 3.8: PL spectra from dots no longer in solution. a) Dots stuck to side-wall. b) Dots fallen to the bottom.

Different examples of PL-spectra from this material are shown in Figure 3.8. As seen, all examples exhibit emission peaked in the 650-regime. To recover emission from material which had dropped out of suspension, a 20 second ultrasonication was performed on a solution which had been etched long enough that emission intensity was very low and both 550-regime and 650-regime peaks were visible. As seen in Figure 3.9 c), an intense signal peaking at about 680 nm immediately appears. With time, the intensity again decreases. Even though a slight shift of the peak is observed, the peak is seemingly pinned in the 650-regime. Subsequent sonications give the same behavior. Thus, the weak, but non-vanishing peak that is often

observed at 650 nm in the PL spectra, seems to come from material that has fallen out of solution. Most of this material falls to the bottom or collects on the sides of the cuvette. However, some small fraction remains in suspension, mostly as agglomerates, due to the

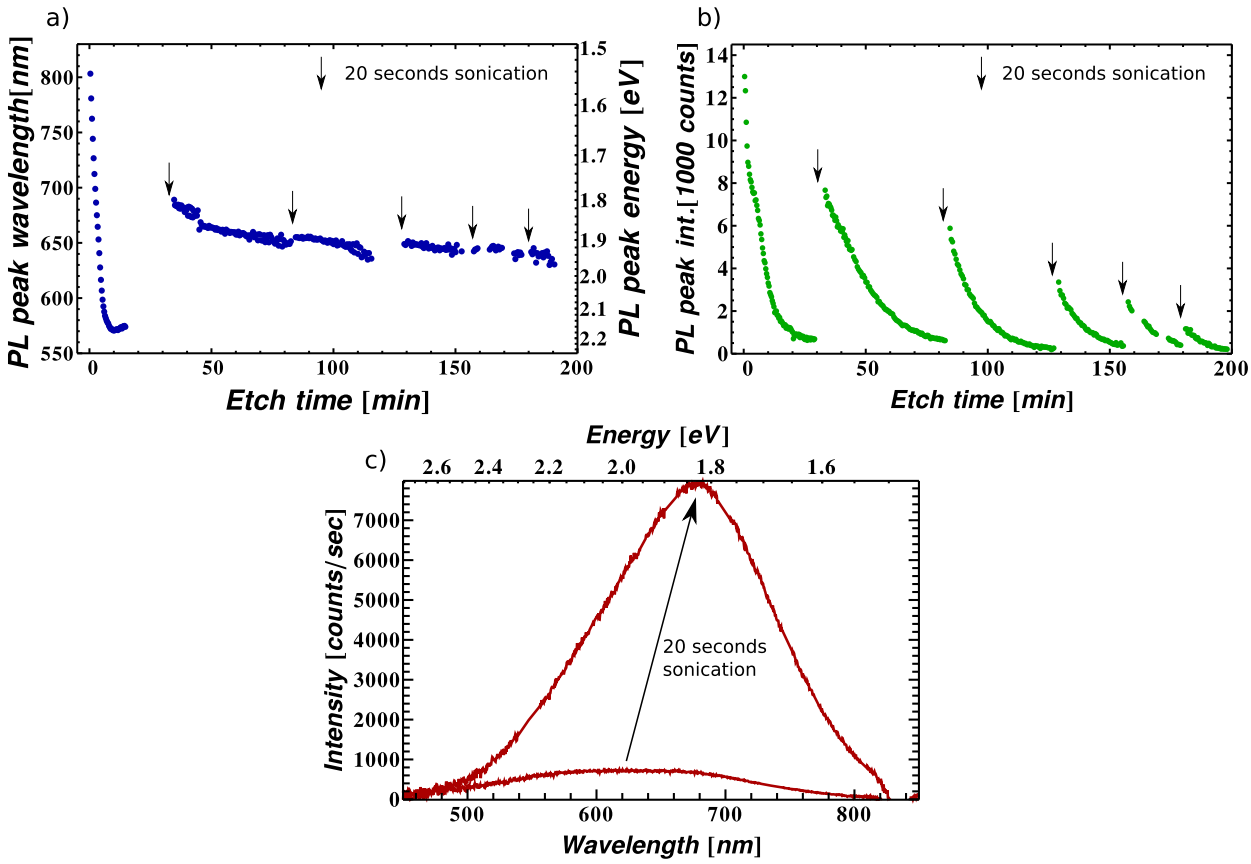

Figure 3.9: Effect of sonication when etching in an aqueous solution of HF and HNO_3. a) Time-evolution of peak wavelength. b) Time evolution of peak intensity. c) In a sample where luminescence had gotten low, 20 seconds sonication immediately led to an intense PL peak centered in the 650-regime. This is explained by the recovery of material that had fallen out of solution.

constant mixing of the stir bar. It is this suspended material that gives rise to the weak 650 nm emission before ultrasonic agitation. The ultrasonic then puts much more of this material back into suspension, strongly enhancing the emission in the 650-regime.

3.2.3 Why do dots fall out of solution?

HF-etching leaves a H-terminated silicon surface [74, 75]. Silicon and hydrogen have very similar electronegativity. Therefore, the surface is non-polar and hence hydrophobic. An oxidized surface, in contrast, is expected to be more hydrophilic. In the etch studied here, strong oxidizing occurs so the dots are likely to have a blend of H-, OH- and O-passivation, similar to what has been observed for bulk Si treated with this etch [76]. Hence the dot surfaces might be expected to have a certain degree of hydrophobicity. Further, in aqueous acidic solutions, Si QDs made by laser pyrolysis are close to their isoelectric point [77]. The aqueous nitric rich etch studied here is strongly acidic, with a pH close to zero. That Si QDs agglomerate and fall out of such a solution is therefore reasonable. However, if material was falling out steadily throughout the etch, one would expect a very broad peak without a well-defined center wavelength. In contrast, the peak after sonication, as well as from the material stuck to the walls or fallen to the bottom, is in these experiments always centered somewhere in the 650-regime. The peaks have a consistent full width at half maximum (FWHM) of about 150 nm or less. These observations are true regardless of where the PL peak wavelength started, i.e. for how long the etch has proceeded before entering into the 650-regime. Further, after the particles are reintroduced to the solution by sonication they do not show significant change in PL peak emission wavelength. This holds also when more, and more concentrated, etchant is added. Another interesting point is that sonication has been performed when the sample still emits at wavelengths longer than 700 nm. No appearance of a 650 nm peak is then observed. However, there is a possibility that the amount of material fallen out at that point is still too low to be detected.

A significant feature in Figure 3.9 is that the intensity recovered right after each sonication is steadily going down with time. Hence, material is not just falling out of the beam-focus and being sonicated back in. Its luminescence signal is somehow bleached. Figure 3.10 shows an experiment where sonication has been done and 650 nm pinning has established. A rapid decrease in intensity is taking place when the sample is being illuminated, while the intensity

stays constant or shows a slight recovery during the periods where the beam is blocked. The degradation in intensity is thus clearly driven by the illumination.

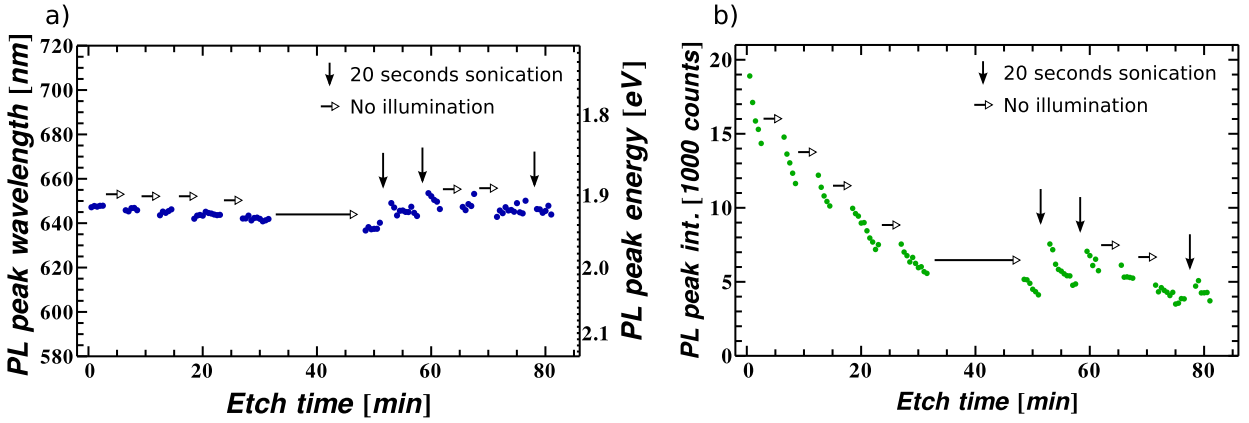

Figure 3.10: Effect of blocking the excitation beam. a) Time-evolution of peak wavelength. b) Time evolution of peak intensity.

Based on the two different classes of photoluminescence in Si QDs described in Section 3.1, two possible models are presented for the behavior just described. These can both potentially explain how the dots preferentially fall out of solution emitting at a certain wavelength, as well as the photodegradation of the signal. A first possibility is that the emission stems from the quantum confined core, and dots start falling out of solution more rapidly at a certain size. Since the etch does not change the dot size further at this point, this explanation need to assume that the dots are sufficiently agglomerated when they fall out that most surfaces are no longer in contact with the etch. Further, UV-light has been shown to introduce non-radiative defects quenching luminescence in Si QDs and p-Si [58, 78–80]. With the etch unable to access the dots and re-passivate the surface, this can explain the photo-induced degradation of the signal. The reason for why the dots preferentially start falling out of solution at a certain size is not immediately clear, but a couple of reasons might be speculated. As the particle size decreases, the diffusion coefficient increases. Hence, the Brownian motion of the dots will become more vigorous, and the dots will more often find themselves in close enough proximity to each other for the short-range van der Waals forces

to cause them to agglomerate [81]. Another possibility is that the oxidation of the surface gets less efficient as the dot size decrease. This would lead to a surface more dominated by H-termination, thus more hydrophobic, and more likely to fall out of solution.

Another explanation can be envisioned where the 650 nm emission comes from a defect state. The degradation of the signal intensity might then come both from photoinduced non-radiative defects, or simply from the dots being etched away. Such an explanation raises a host of other questions. Why does all the material falling out of solution have the same defect state, while the material still in solution does not? Is the defect the reason why the dots fall out, or is the defect created when the dots are no longer in solution and/or illuminated? And why do dots with such a defect not occur in the early stages of the etch? A change from core- to defect-emission in Si QDs as they get smaller have been observed before. An explanation was initially proposed by Wolkin et al., where trap states introduced by the presence of Si=O-bonds on the surface would lead to a step-wise pinning of the hole and electron energy levels [55]. This would ultimately prevent the PL peak energy from further increase as the dots get smaller than a certain limit. Several later studies have observed similar behavior, where the PL deviates from theoretical predictions as the dot size goes below $\sim$ 2.9 nm [50, 82, 83]. A refinement of Wolkin's model was later put forward by Martin et al. based on single-dot spectroscopy experiments [84]. They proposed that the localization is driven by strong coupling of the electron and hole to Si-O-Si phonons. These effects were seen in the same wavelength range as the pinning behavior observed in this study. Consequently, it should be considered as a possible explanation for this phenomena. All the studies referenced above emphasize the role of oxygen on the surface of the QDs. During etching, a competition between oxidation of the surface and removal of oxygen by HF is occurring. This will, as pointed out in the beginning of this section, lead to dot surfaces having a mixture of H-, OH- and O- passivation during the experiment. In addition, theoretical studies predict that the barrier to formation of Si=O groups from a Si-OH bond by photo-excitation can be overcome by the excitation source used here [85]. Thus the formation of defect states associated with

oxygen can be rationalized. The pinning behavior might then represent a transition from core luminescence to defect luminescence. If so, why is this predominantly occurring in material fallen out of solution? Having oxygen species on the surface should lead to the surface having a more hydrophilic character leading to better dissolution. A more likely explanation within this model is that the defects are introduced after the material has fallen out, as the HF is no longer efficient at removing surface oxide.

3.2.4 Role of the solvent

When etching nanostructured silicon, different alcohols are commonly used as a wetting agent [33, 73, 86]. It is therefore a reasonable hypothesis that addition of an alcohol such as ethanol will help keep the dots in solution. This gives several pronounced effects. As

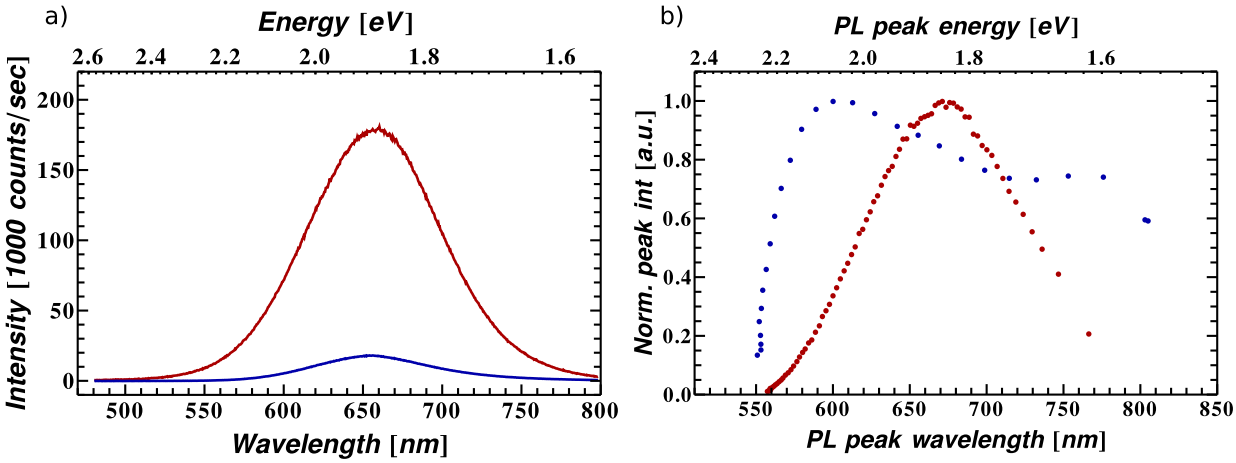

Figure 3.11: Absolute intensity and intensity variation when etching in water-based vs. ethanol-based solutions. a) Example of difference in luminescence signal when etching in an ethanol-based solution (Red) and in a water-based solution (Blue). A comparable amount of SiQDs is used. b) Example of typical intensity development with blue-shifting of PL when etching in an ethanol-based solution (Red) and in a water-based solution (Blue).

seen in Figure 3.11 a), the use of 50 % ethanol in the etch mixture gives a clearly evident enhancement of the luminescence intensity. The etch rate also slows down significantly, by about a factor of four compared to etching with the dots dissolved in just water. In the remainder of this thesis etching with HF/HNO_3 in a solution containing only water will for

simplicity be referred to as etching in a "water-based solution", while etching in a solution of 50% water/50% ethanol will be referred to as etching in an "ethanol-based solution".

Figure 3.12 shows an experiment where sonication is performed on a sample etched in an ethanol-based solution. It is seen that even when adding ethanol to the etch mixture, there is still a significant amount of material falling out. However, comparing the recovered intensity to the maximum intensity, it seems to be less material falling out than when etching in a water-based solution. This is further supported by inspection of the cuvette under UV-illumination, where less material is observed clinging to the walls, floating on the surface and fallen to the bottom. Again the redispersed material emits in the 650-regime, but in

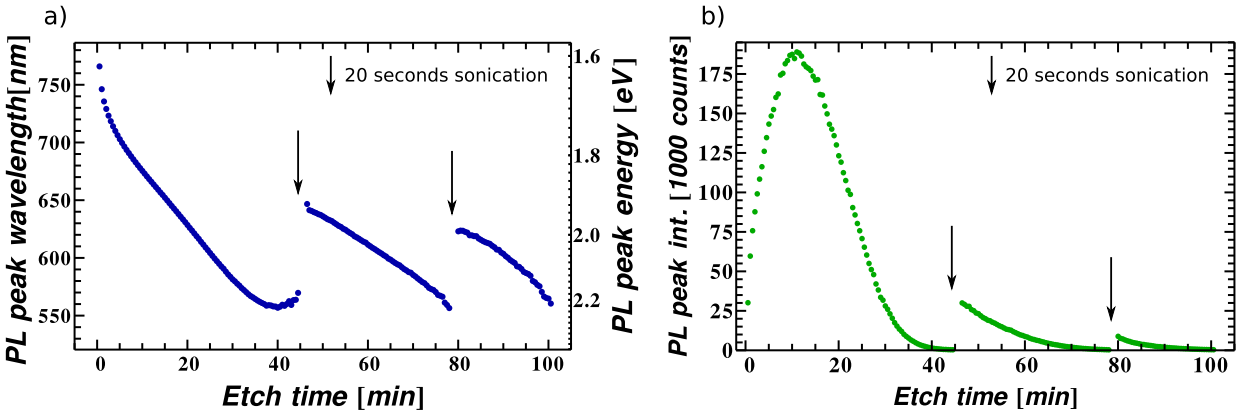

Figure 3.12: Effect of sonication when etching in an ethanol-based solution. a) Time-evolution of peak emission wavelength. b) Time evolution of peak intensity.

contrast to when etching in a water-based solution (Figure 3.9 a)), the recovered emission blue-shifts (Figure 3.12 a)). It is also seen that subsequent sonications recover emission at shorter wavelengths. It can be argued that the dots are easier to redisperse into the ethanol mix than into pure water, and that this lets the dots again be exposed to the etch. This supports a model where the emission stems from exciton recombination in the core, and the 650-pinning is due to dots being more likely to agglomerate and fall out of solution below a certain size.

The intensity development is also significantly different when ethanol is used. This is most easily seen when the peak intensity is normalized, and plotted against peak wavelength

as in Figure 3.11 b)[12]. However, from the results presented in the preceeding sections, it is reasonable to assume that several mechanisms are present that influence the observed development in intensity, both when etching in water-based and ethanol-based solutions. One involves the dots falling out of solution, and one involves the intensity degrading by UV-illumination. These two might be interrelated, and are in addition superimposed on the actual intensity variation coming from the dots getting smaller. With so many factors involved, it is hard to draw any conclusions based on the observed variation in intensity alone. However, assuming that dots that have fallen out are not coming back into solution (except when sonicated), the observed increases in intensity must be "real", in the sense that they represent variations coming from changes in the QDs themselves, and not from whether they stay in solution or not. Experiments to probe these effects more reliably will be proposed in Chapter 4.

3.2.5 Stabilization of dots in solution

Zeta-potential and thereby colloidal stability is commonly tuned by changing the pH and/or the ionic strength of the solution. Zeta-potential measurements of Si QDs suggests that higher pH would be better for stable suspensions [77]. In experiments to obtain samples for TEM analysis, etching was performed in 5 % HF and no HNO_3, as will be discussed in Section 3.3[13]. Using only HF, material falling out of solution is still observed, but the increase in intensity caused by sonication is an order of magnitude less, relative to the maximum intensity, than when HNO_3 is also present. This points towards more material staying in solution. Explanations such as different surface passivation with the presence of HNO_3 might be suggested. However, in light of the referenced trend in zeta-potential, it is interesting to note that the HF solution used has a pH of about 4, compared to the standard HF/HNO_3

[12]The development in intensity presented for etching in an ethanol-based solution is very reproducible. This is not the case when etching in a water-based solution, even though a development as the one presented in Figure 3.11 b) have been observed multiple times.

[13]Using only HF causes a blue-shift of the PL-peak emission wavelength very similarly to using a HF/HNO_3 mix. Thus the oxidation due to water and UV-illumination can fully replace the effect of HNO_3, in line with the discussion in Section 3.2.1.

mix, with a pH close to zero. This result suggests future studies examining adjustment of the pH as a possible way of making the dots stay in solution. However, since altering the pH will change the surface properties of the dots (as will any attempt of stabilization of the dots in solution), careful attention must be paid to how this might change the etching characteristics.

3.2.6 The 550 nm limit

A question that arises after the preceeding discussion is how the material's lack of ability to stay in solution is related to the limiting emission wavelength behavior seen in the 550-regime (in contrast to the 650-regime which is clearly connected to the material that leaves solution). Are the dots falling out of solution and this phenomena connected? The answer to this seems to be no. No peak emission at 550 nm is ever observed from material clinging to the walls nor fallen to the bottom. Emission in this wavelength range is also not recovered upon sonication. Therefore, another mechanism for this behavior must be sought. Through the in-situ etch experiments, it is seen that the limit at $\sim$ 550 nm to where the signal dies away is remarkably consistent. Within the region of parameter space explored in this study, it seems independent of solvent (water, water/ethanol, water/methanol), etchant mixing ratios (see Figure 3.13), sample concentration (0.01 mg/ml to 0.15 mg/ml), excitation wavelength (365 nm and 458 nm) and excitation power (0.18 mW and 1.5 mW for 365 nm). Even with indications that more material is staying in solution when adding a wetting agent, as well as when changing pH, the 550 nm limit remains. The presence of this limit using different etchant mixing ratios and sample concentrations, as well as when more etchant is added during the experiment, further shows that it is not connected to depletion of any of the etchant constituents.

It has been shown several times in this study that the illumination by UV-light has pronounced effects on the change in luminescence properties of the Si QDs. In that respect, an interesting observation was done by Hua et al. [66]. When illuminating particles with 355-nm light, they saw a photo-bleaching that was very rapid for green-emitting particles,

significantly slower for yellow-emitting particles, and hardly observable for red-emitting particles. I.e. the photo-bleaching was more rapid for smaller particles. Further, Godefroo et al. suggested that UV-light is preferentially introducing defects in smaller nanocrystals, as they tend to be more strained due to higher surface curvature[58]. A possible explanation to the 550-limit is then that the dots reach a size where degradation of the PL due to the UV-light rapidly speeds up. However, since the same 550-limit is observed when illuminating with 458 nm light, the threshold energy for photo-bleaching must be less than 2.9 eV.

To gain more information about this behavior, as well as about why dots seemingly fall out at a certain size, the study needs to be extended to other measurement techniques. A TEM and a PLE study will be discussed in the following sections. Additional techniques of interest that were not feasible within the time frame of this study will be discussed in Chapter 4.

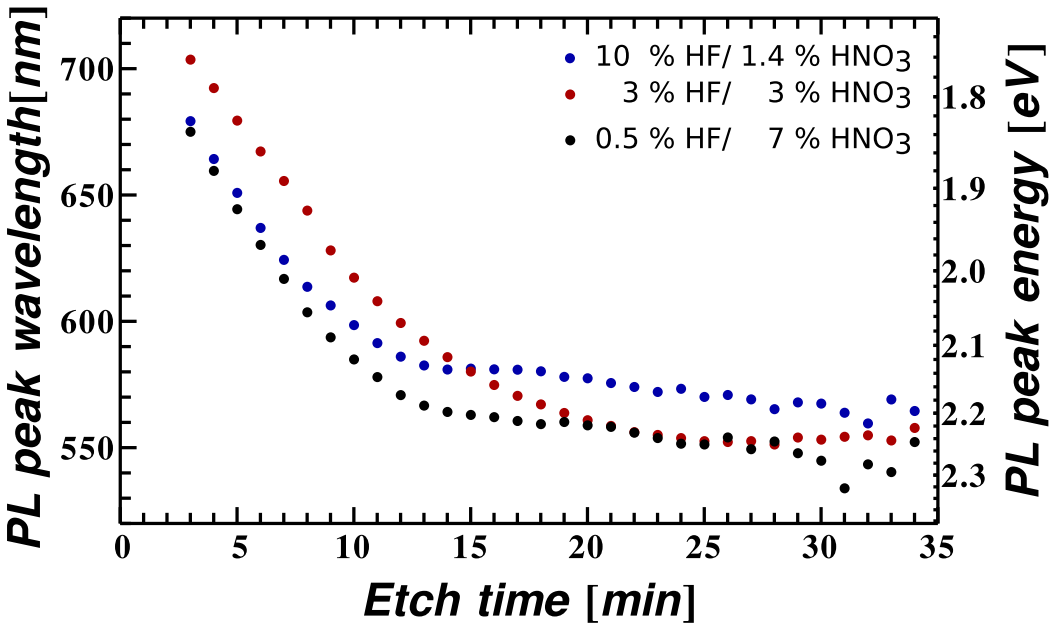

Figure 3.13: Etching with different HF to HNO_3 concentration ratios. The same initial sample was divided in three and etched with different mixing ratios of HF and HNO_3 in water. All etches behaved similar, both with regard to etch rate and pinning behavior.

3.3 Does the size change?

The blue-shift of the PL during the early stages of the etch points toward the dots becoming smaller. Using TEM to directly observe this was explored. For reasons discussed below there was too much uncertainty in the size distributions to draw any conclusions. During the course of the study, however, techniques were developed and observations made that will be useful in future work, hence this study will be discussed in the following.

To prepare dots from the etching solution for transmission electron microscopy (TEM) analysis, a method was needed to remove parts of the material from the solution at given points during the etch. Centrifugation and extraction by adding a solvent which is immiscible with water, but in which the dots are more soluble (solvent extraction) were tested [27, 87]. Within the experiments of this study however, the method giving the best results turned out to be the simplest[14]. A drop of the etching solution was placed directly on a holey carbon TEM grid and the liquid was evaporated in a vacuum chamber. For this, the etching was performed in 5% HF only, as the nitric acid was expected to attack the carbon on the grid. Using this method, samples were taken out of the etch solution for TEM-analysis at different points during the blue-shifting of the PL emission wavelength.

Imaging of the etched particles was more difficult relative to other unetched silicon quantum dot samples grown by PECVD that were previously studied [88]. This was both in terms of contrast, selected area electron diffraction (SAED) patterns, and lattice fringing. It is likely that a contributing reason for this was that the particles were covered in a sheathing that are not normally seen when imaging other dots. A possible origin of this sheathing is that the HF is somehow attacking and dissolving parts of the grid, even with no HNO_3 in the solution. That such an attack of the grid took place was supported by the observation of unusual deformation of the grid both by eye and in TEM imaging. Because of

[14]This does not mean that solvent extraction and centrifugation can be ruled out as possible methods for sample preparation. These have been succesfully used by others, and further exploration and tailoring of these techniques to the system studied here might give better results than what was achieved in these initial attempts.

these issues in image acquisition, sizes were measured on images taken in the bright field on non-fringing particles, which is not ideal. Varying degrees of agglomeration were also observed throughout the samples[15]. In large regions with significant agglomeration, this made it hard to discern the particle-edges and to reliably sample a representative distribution of the particles present. Therefore, the errors in the acquired size distributions were large, and no conclusions could be drawn as to whether the size was changing or not. Future strategies to obtain more reliable data from TEM will be discussed in Chapter 4.

Finally, it should be noted that good SAED patterns and images of particles showing lattice fringes were possible to obtain in a few areas. These show good agreement with expected patterns for Si, as shown in Figure 3.14. Some dark field images were acquired by picking out single diffraction planes from the SAED-patterns, but the number of counts achievable from these were too low to provide any additional information.

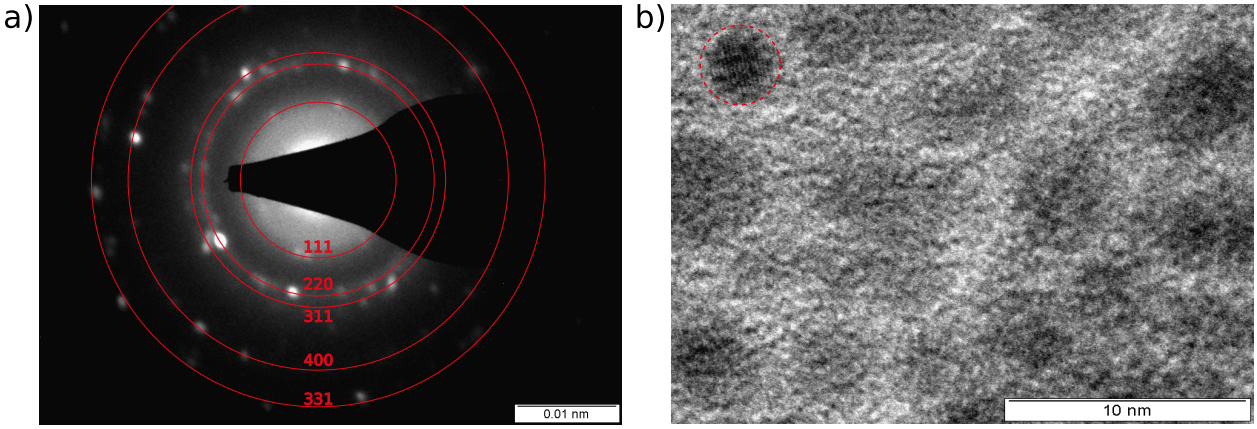

Figure 3.14: Example of nice SAED pattern and particle showing lattice fringing. a) Rings in SAED pattern matches up with silicon. b) Particle show lattice fringes corresponding to the (220)-lattice plane.

[15]In addition, some bigger and more unidentifiable pieces of matter, with sizes of >50 nm were observed. These did not show any sign of faceting nor fringing, thus it is doubtful that they were large crystalline particles. It is reasonable that these larger "particles", together with big agglomerates, are the main origin of the scattering indicated by observations using other measurement techniques such as PL (Section 2.4.2), PLE (Section 3.4) and dynamic light scattering (DLS). DLS was attempted as an alternative way of attaining size distributions. To get reasonable results proved difficult, most likely due to the presence of large scatterers in solution. Therefore, the DLS-study is not included in this thesis.

3.4 In-situ photoluminescence excitation experiments

Because of the superior signal strength, as well as the reproducibility of the PL-peak evolution when etching, PLE was performed etching in an ethanol-based solution. The blue-shifting of the PL emission wavelength with increasing etch-time was monitored by acquiring PL spectra at regular time-intervals. Alternating with PL measurements, PLE spectra were acquired, with the emission detection wavelength chosen as the peak wavelength of the last PL spectrum. In this way, absorption of the dots were measured as they changed their PL emission wavelength from 740 nm to 510 nm[16].

PLE spectra at different emission detection wavelengths are shown in Figure 3.15 a). There is a long wavelength range from the detection energy before any appreciable absorption is taking place. This is commonly seen for Si QDs and p-Si, and is a result of the very low joint density of states near the band-edge [89]. As the excitation wavelength moves into the UV, the absorption increases significantly, and a sharp and distinct peak is seen at about 340 nm ($\sim$3.65 eV). Such a peak somewhere between 280 and 360 nm is frequently seen in PLE spectra for Si nanocrystals [25, 27, 51, 90–92]. Occurrence of enhanced absorption in this region can be related to the direct-gap absorption region of bulk Si from 3.4 to 4.4 eV [47, 93], as is often done in the literature [90–92]. Such an explanation is reasonable, as it has been shown that Si nanocrystals can maintain a band structure with bulk-like character down to about 2 nm [94]. What is poorly addressed in the literature is why the absorption dies off at higher energies[17]. For Si nanocrystals where both PLE and absorption have been measured and compared [25, 27, 51, 90–92], the absorption continues to increase as one moves to higher energies, while the PLE signal exhibits a peak similar to the one observed in this study. It is not clear why absorption at higher energies should not lead to a PL signal. The

[16]The emission wavelength of the PL peak did as before get pinned in the 550-regime. However, probing the high energy tail of the pinned PL peak allowed acquiring PLE spectra with emission detection wavelengths down to 510 nm.

[17]Measurements at even higher energies than showed here is not possible due to strong absorption from the cuvette in this region. There is also some absorption from the cuvette at wavelengths between 300 and 400 nm, but this has been corrected for in all spectra included here.

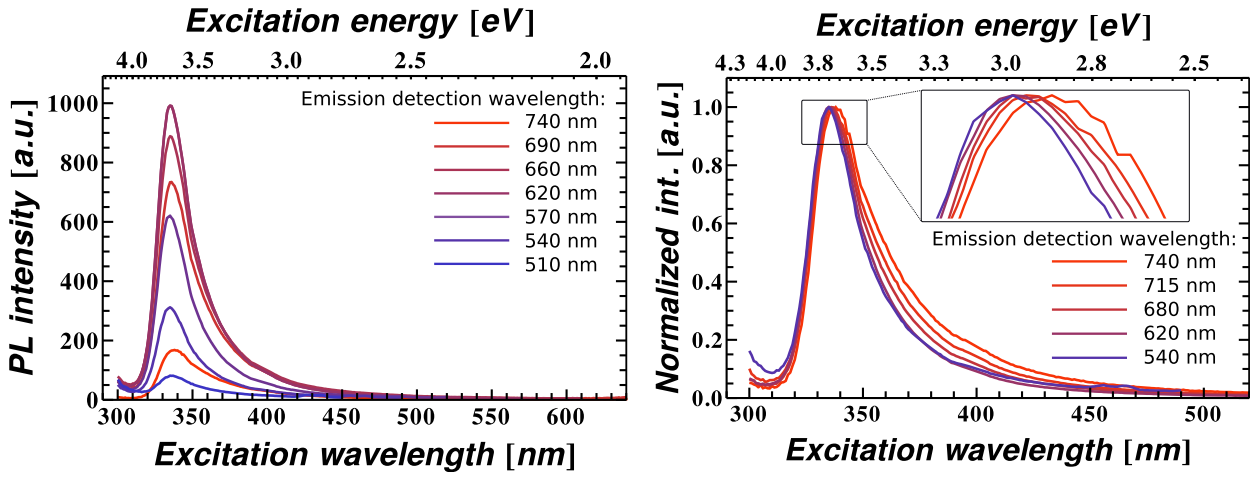

Figure 3.15: PLE spectra at different emission detection wavelengths. a) The intensity variations with different emission detection wavelengths follows the variation in PL intensity throughout the etch. The shape of the spectra remains practically the same. b) Example of normalized PLE spectra. Inset: A slight blue shift in the peak wavelength can be seen as the etch proceeds, the size decreases, and the emission detection energy is increased to match the shift in peak emission.

results presented here do not contribute new information to explain this behavior, but do contribute well controlled and reproducible evidence that such a peak in the PLE spectrum occurs. Also, most other studies report PLE measurements from dots of one size. Here, the same population of dots is measured at different sizes, and the peak in the PLE spectrum is consistently present.

Naturally, the intensity variation in the spectra in Figure 3.15 a) follows the variation with emission peak wavelength in the PL signal as seen earlier(Figure 3.11 b)). Further, the shape of the spectra remains largely unchanged. However, a slight blue shift of the peak wavelength is observed, which is more easily seen when the spectra are normalized (Figure 3.15 b), inset). As the dots are etched smaller, and the emission detection wavelength is shifted accordingly from 740 nm to 510 nm, the PLE-peak is fairly steadily blue-shifted from about 338 nm to 334 nm. Thus, accompanying a blue-shift in the PL emission wavelength of about 750 meV, the peak in the PLE spectrum is only shifted by 40 meV. This agrees reasonably well with findings for porous silicon by Ben-Chorin et al. For a similar

change in the PL detection energy, they show a blue-shift of about 50-60 meV for the energy they assign to the first direct transition in the bandgap, $\Gamma_{25} \rightarrow \Gamma_{15}$ [47]. This transition is the onset of the direct gap absorption region that is often put forward as the reason for the peaking in the PLE-spectra, as discussed above. The PL peak on the other hand, is related to the lowest energy indirect gap, $\Gamma_{25} \rightarrow \Delta_1$[18]. Thus associating the peaks in the PLE and PL spectra to the $\Gamma_{25} \rightarrow \Gamma_{15}$ and $\Gamma_{25} \rightarrow \Delta_1$ transitions, respectively, the observed blue-shifts indicate a much larger effect of quantum confinement on the indirect gap. This is consistent with the conclusions in both the work of Ben-Chorin et al., as well as other studies [94, 95]. Contrary to this, however, a small red-shift of the first direct gap in this region have been observed both experimentally[92], and in empirical pseudopotential calculations [96]. It can also not be ruled out that the blue-shift is just an artifact of the measurement. Thus, a final conclusion as to the origin of the observed blue-shift cannot be made, but this observation adds to a body of work showing that the higher energy transitions are significantly less (if at all) affected by quantum confinement than the gaps lower in the band structure.

A change in size with etching should result in a change in absorption onset, reflecting the change in the lowest energy gap in the band structure. Due to the indirect nature of this gap in Si, such an onset is hard to observe. Contrary to observations for direct gap QDs such as CdSe and InAs, no excitonic peaks are seen in the absorption spectra. In the system presented here, scattering enlarged the excitation line width so that moving close to the emission detection wavelength was difficult. This effectively hindered any observation of an absorption onset.

Finally, a PLE spectrum was acquired from material that had fallen out of solution, thus emitting in the 650-regime, directly after recovery of the PL signal by sonication. The spectrum is identical, thus not blue-shifted, to spectra from material staying in solution, emitting around 650 nm. If one assumes that the wavelength of the peak can be taken as

[18]These can not be related one to one, since a size dependent Stokes shift is most likely involved. An attempt of a quantitative treatment of this can be found in [47]. Qualitatively however, a blue-shift for the $\Gamma_{25} \rightarrow \Delta_1$ energy is accompanied by a blue-shift in the PL peak emission wavelength related to recombination of quantum confined carriers.

an indication of degree of confinement, as discussed above, this would indicate that the sizes are the same for dots emitting at 650 nm both if they are staying in, or have fallen out of solution. Thus this further supports the model where dots preferentially fall out at a certain size.

CHAPTER 4
CONCLUSIONS AND FUTURE WORK

The work of this thesis has shown that the study of the effect of a wet-chemical etch on Si QDs can be performed in-situ. Photoluminescence from the same ensemble of Si QDs was followed in real time as it was etched, resulting in a blue-shift of the PL emission wavelength over a range of more than 250 nm. Both this blue-shift and the variation in PL peak intensity in the first part of the etch was consistent with emission from quantum confined carrier recombination. The developed experiment setup allowed for close monitoring of changes in etching conditions, and this was used to show that the etch is photoassisted. Further, it was shown that addition of ethanol as a wetting agent to the etching mixture leads to a significant enhancement of PL intensity.

Two distinct regimes where the PL peak emission wavelength becomes pinned and cannot be changed any further were identified, at 520-560 nm and at 620-680 nm. Pinned PL peak emission in the 650-regime was shown to originate from material fallen out of solution. Further, it was shown that the degradation of the PL emission from this material was largely driven by the UV-illumination. At emission wavelengths that lie within this wavelength range, a transition from quantum confined exciton related emission to defect related emission has been reported multiple times in the literature for Si QDs. Such a transition makes a plausible explanation for the pinning behavior. However, when material emitting in the 650-regime was redispersed in the solution by sonication, a further blue-shift towards 550 nm was sometimes observed, which might not be expected if emission originated from a defect related transition. The PLE spectra from material emitting in the 650-regime were also indistinguishable to spectra from particles staying in solution. These observations indicate that the emission from the material falling out of and staying in solution is similar in nature. In turn, this means that emission in the 650-regime is due to material preferentially falling

out at or below a certain size. Different explanations for this were discussed, but a further exploration into the colloidal chemistry of the solution should be pursued. Experiments in this study indicated that a possible route to stabilize the dots in solution would involve a careful study of the effect of pH. Since it was shown here that the etching process occurs in solutions only containing HF and solvent, a viable approach would be to control the pH by buffering this solution using NH_4F[19]. pH can further be tuned over a wider range by addition of HCl or NH_4OH [97].

For the 550-regime, nothing was found to indicate that this pinning is due to material that easily precipitates out of solution. This regime corresponds very well with the high energy limit for blue-shifting of PL emission wavelength presented in other studies. The presented experiments showed that this pinning-behavior is an inherent effect of the etching process. Within the experiments of this study the limit was independent of solvent, etchant mixing ratio, sample concentration, excitation energy and excitation power. How the limit could be related to photo-bleaching being more prominent in smaller dots was discussed. If this is the case, it would mean that there are still dots in solution when the emission has vanished in the 550-regime, they have just turned "dark". Therefore, an attempt to recover the luminescence could potentially be made. Attaching different surface ligands to Si QDs has been shown to significantly enhance the PL, which can in large be attributed to passivation of non-radiative defects [90, 98, 99]. Therefore, to perform a ligand attachment procedure such as hydrosilylation on a sample where emission has vanished in the 550 region might be interesting. Given that the photo-bleaching hypothesis is correct, and the photo-induced defects do not hinder the ligand attachment reaction, this might be a method to recover PL emission from these dots.

A key to understanding these phenomenas is to determine whether the nature of the PL emission changes when the different pinning behaviors occur. Therefore a study of the time-resolved PL (TRPL) will be useful. Since etching in a solution based on ethanol and

[19]Such an etch is routinely used in the silicon processing industry.

water was shown to give reproducible results with very good signal intensity, this should be achievable. An in-situ TRPL study is therefore seen as a promising future direction. The same holds for a study of the quantum yield. If a lifetime study indicates that one or both of these pinnings are related to the formation of a defect, an in-situ electron spin resonance (ESR) study might be able to provide supporting and supplementary information in this regard.

Absorption measurements for the ensemble of dots as they were etched smaller were successfully obtained through PLE experiments. These supported several other studies showing that quantum confinement has a much smaller impact on the first direct gap in the silicon band structure than on the lower energy indirect gap.

Attempts were made at obtaining size-distributions for the particles by TEM. This was not successful, probably in part due to the current procedure of sample preparation for TEM-analysis. A further exploration into different extraction techniques that might be more suitable for TEM sample preparation is therefore suggested. Further, based on the observation of big agglomerates in TEM, an attempt to purify the starting sample by separating out these big pieces of matter, if present before etching, might prove beneficial. This would shed light on whether the big agglomerates form during the etching process, or are present all along. If this could also result in a reduction of the observed scattering, it would be advantageous for the optical measurements, more specifically the chance of observing an absorption onset. Combined with a better understanding of how to keep the dots from falling out of solution, this might further turn out to be what is needed for successful extension of the study to include dynamic light scattering (DLS) experiments. In this technique, the occurence of larger particles and agglomerates in solution will overwhelm smaller scatterers, making it very difficult to observe particles in the size-range studied here. If this can be avoided, DLS represents an intriguing opportunity to follow a size change in real time.

One of the goals of this study was to investigate whether wet-chemical etching is a feasible route to producing Si QDs with sizes less than 2 nm. Such a material could have

significant impact for several technologies, including photovoltaics. While etching can be used to change the size substantially, and the size clearly approaches the desired size range, it has not entered it. Hence a conclusion on this issue has not been reached. However, a better understanding of the etching and the parameters that affects it has been obtained. Combined with the in-situ measurement techniques that have constantly been improved and developed throughout this work, this provides a good foundation for further exploration.

REFERENCES CITED

[1] The International Energy Agency. World Energy Outlook, Executive Summary. http://www.iea.org/publications/freepublications/publication/, 2012.

[2] The Intergovernmental Panel on Climate Change. Climate Change 2007, Synthesis Report. http://www.ipcc.ch/publications_and_data/publications_ipcc_fourth_assessment_report_synthesis_report.htm, 2007.

[3] Nathan S. Lewis George W. Crabtree. Solar Energy Conversion. *Physics Today*, 60:37–, 2007.

[4] George W. Crabtree Jeff Tsao, Nate S. Lewis. Solar FAQs. http://www.sandia.gov/~jytsao/, 2006.

[5] Martin A.Green. *Solar Cells*. Prentice-Hall, Inc., Englewood Cliffs, N.J., 1982.

[6] David Ginley, Reuben Collins, and Martin Green. Solar Energy Conversion Toward 1 Terrawatt. *MRS Bulletin*, 33(April):355–364, 2008.

[7] Octavi E. Semonin, Joseph M. Luther, and Matthew C. Beard. Quantum dots for next-generation photovoltaics. *Materials Today*, 15(11):508–515, November 2012. ISSN 13697021. doi: 10.1016/S1369-7021(12)70220-1. URL http://linkinghub.elsevier.com/retrieve/pii/S1369702112702201.

[8] William Shockley and Hans J. Queisser. Detailed Balance Limit of Efficiency of p-n Junction Solar Cells. *Journal of Applied Physics*, 32(3):510, 1961. ISSN 00218979. doi: 10.1063/1.1736034. URL http://link.aip.org/link/JAPIAU/v32/i3/p510/s1&Agg=doi.

[9] National Renewable Energy Laboratory. Solar Technologies Market Report. (http://www.nrel.gov/docs/fy12osti/51847.pdf, 2010.

[10] The International Energy Agency. Solar Photovoltaic Roadmap. http://www.iea.org/publications/freepublications/publication/, 2012.

[11] MA Green and Keith Emery. Solar cell efficiency tables (version 39). *Progress in ...*, (version 39):12–20, 2012. doi: 10.1002/pip. URL http://onlinelibrary.wiley.com/doi/10.1002/pip.2163/full.

[12] A J Nozik, M C Beard, J M Luther, M Law, R J Ellingson, and J C Johnson. Semiconductor quantum dots and quantum dot arrays and applications of multiple exciton generation to third-generation photovoltaic solar cells. *Chemical reviews*, 110(11):6873–90, November 2010. ISSN 1520-6890. doi: 10.1021/cr900289f. URL http://www.ncbi.nlm.nih.gov/pubmed/20945911.

[13] A.J Nozik. Quantum dot solar cells. *Physica E: Low-dimensional Systems and Nanostructures*, 14(1-2):115–120, April 2002. ISSN 13869477. doi: 10.1016/S1386-9477(02)00374-0. URL http://linkinghub.elsevier.com/retrieve/pii/S1386947702003740.

[14] D. S. Boudreaux, F. Williams, and A. J. Nozik. Hot carrier injection at semiconductor-electrolyte junctions. *Journal of Applied Physics*, 51(4):2158, 1980. ISSN 00218979. doi: 10.1063/1.327889. URL http://link.aip.org/link/JAPIAU/v51/i4/p2158/s1&Agg=doi.

[15] Octavi E Semonin, Joseph M Luther, Sukgeun Choi, Hsiang-Yu Chen, Jianbo Gao, Arthur J Nozik, and Matthew C Beard. Peak external photocurrent quantum efficiency exceeding 100% via MEG in a quantum dot solar cell. *Science (New York, N.Y.)*, 334 (6062):1530–3, December 2011. ISSN 1095-9203. doi: 10.1126/science.1209845. URL http://www.ncbi.nlm.nih.gov/pubmed/22174246.

[16] Zhibin Lin, Alberto Franceschetti, and Mark T Lusk. Size dependence of the multiple exciton generation rate in CdSe quantum dots. *ACS nano*, 5(4):2503–11, April 2011. ISSN 1936-086X. doi: 10.1021/nn200141f. URL http://www.ncbi.nlm.nih.gov/pubmed/21355556.

[17] National Renewable Energy Laboratory. Research Cell Efficiency Records. http://www.nrel.gov/ncpv/, 2013.

[18] Matthew C Beard, Kelly P Knutsen, Pingrong Yu, Joseph M Luther, Qing Song, Wyatt K Metzger, Randy J Ellingson, and Arthur J Nozik. Multiple exciton generation in colloidal silicon nanocrystals. *Nano letters*, 7(8):2506–12, August 2007. ISSN 1530-6984. doi: 10.1021/nl071486l. URL http://www.ncbi.nlm.nih.gov/pubmed/17645368.

[19] L Mangolini, E Thimsen, and U Kortshagen. High-yield plasma synthesis of luminescent silicon nanocrystals. *Nano letters*, 5(4):655–9, April 2005. ISSN 1530-6984. doi: 10.1021/nl050066y. URL http://www.ncbi.nlm.nih.gov/pubmed/15826104.

[20] Melanie L. Mastronardi, Eric J. Henderson, Daniel P. Puzzo, and Geoffrey A. Ozin. Small Silicon, Big Opportunities: The Development and Future of Colloidally-Stable Monodisperse Silicon Nanocrystals. *Advanced Materials*, pages n/a–n/a, August 2012. ISSN 09359648. doi: 10.1002/adma.201202846. URL http://doi.wiley.com/10.1002/adma.201202846.

[21] Zhibin Lin, Huashan Li, Alberto Franceschetti, and Mark T Lusk. Efficient exciton transport between strongly quantum-confined silicon quantum dots. *ACS nano*, 6(5): 4029–38, May 2012. ISSN 1936-086X. doi: 10.1021/nn3003407. URL http://www.ncbi.nlm.nih.gov/pubmed/22468899.

[22] Sabrina Niesar, Rui N. Pereira, Andre R. Stegner, Nadine Erhard, Marco Hoeb, Andrea Baumer, Hartmut Wiggers, Martin S. Brandt, and Martin Stutzmann. Low-Cost Post-Growth Treatments of Crystalline Silicon Nanoparticles Improving Surface and Electronic Properties. *Advanced Functional Materials*, 22(6):1190–1198, March 2012. ISSN 1616301X. doi: 10.1002/adfm.201101811. URL http://doi.wiley.com/10.1002/adfm.201101811.

[23] Huashan Li, Mark T Lusk, Reuben T Collins, and Zhigang Wu. Optimal size regime for oxidation-resistant silicon quantum dots. *ACS nano*, 6(11):9690–9, November 2012. ISSN 1936-086X. doi: 10.1021/nn303109t. URL http://www.ncbi.nlm.nih.gov/pubmed/23061893.

[24] Martin A Green, Jianhua Zhao, Aihua Wang, Peter J Reece, and Michael Gal. Efficient silicon light-emitting diodes. *Nature*, 412(August):805–808, 2001.

[25] Folarin Erogbogbo, Ken-tye Yong, Indrajit Roy, Gaixia Xu, Paras N Prasad, and Mark T Swihart. Biocompatible Luminescent Silicon. *ACS nano*, 2(5):873–878, 2008.

[26] L Pavesi, L Dal Negro, C Mazzoleni, G Franzò, and F Priolo. Optical gain in silicon nanocrystals. *Nature*, 408(6811):440–4, November 2000. ISSN 0028-0836. doi: 10.1038/35044012. URL http://www.ncbi.nlm.nih.gov/pubmed/11100719.

[27] Melanie L Mastronardi, Frank Hennrich, Eric J Henderson, Florian Maier-Flaig, Carolin Blum, Judith Reichenbach, Uli Lemmer, Christian Kübel, Di Wang, Manfred M Kappes, and Geoffrey A Ozin. Preparation of monodisperse silicon nanocrystals using density gradient ultracentrifugation. *Journal of the American Chemical Society*, 133(31):11928–31, August 2011. ISSN 1520-5126. doi: 10.1021/ja204865t. URL http://www.ncbi.nlm.nih.gov/pubmed/21740050.

[28] Amane Shiohara, Sanshiro Hanada, Sujay Prabakar, Kohki Fujioka, Teck H Lim, Kenji Yamamoto, Peter T Northcote, and Richard D Tilley. Chemical reactions on surface molecules attached to silicon quantum dots. *Journal of the American Chemical Society*, 132(1):248–53, January 2010. ISSN 1520-5126. doi: 10.1021/ja906501v. URL http://www.ncbi.nlm.nih.gov/pubmed/20000400.

[29] R W Liptak, B Devetter, J H Thomas, U Kortshagen, and S a Campbell. SF6 plasma etching of silicon nanocrystals. *Nanotechnology*, 20(3):035603, January 2009. ISSN 1361-6528. doi: 10.1088/0957-4484/20/3/035603. URL http://www.ncbi.nlm.nih.gov/pubmed/19417298.

[30] A A Seraphin, E Werwa, and K D Kolenbrander. Materials research. *Journal of Materials Research*, 12(12):3386–3392, 1997.

[31] L. T. Canham. Silicon quantum wire array fabrication by electrochemical and chemical dissolution of wafers. *Applied Physics Letters*, 57(10):1046, 1990. ISSN 00036951. doi: 10.1063/1.103561. URL http://link.aip.org/link/APPLAB/v57/i10/p1046/s1&Agg=doi.

[32] Xuegeng Li, Yuanqing He, SS Talukdar, and MT Swihart. Process for preparing macroscopic quantities of brightly photoluminescent silicon nanoparticles with emission spanning the visible spectrum. *Langmuir*, (15):8490–8496, 2003. URL http://pubs.acs.org/doi/abs/10.1021/la034487b.

[33] Anoop Gupta, Mark T. Swihart, and Hartmut Wiggers. Luminescent Colloidal Dispersion of Silicon Quantum Dots from Microwave Plasma Synthesis: Exploring the Photoluminescence Behavior Across the Visible Spectrum. *Advanced Functional Materials*, 19(5):696–703, March 2009. ISSN 1616301X. doi: 10.1002/adfm.200801548. URL http://doi.wiley.com/10.1002/adfm.200801548.

[34] Keisuke Sato, Hiroaki Tsuji, Kenji Hirakuri, Naoki Fukata, and Yusuke Yamauchi. Controlled chemical etching for silicon nanocrystals with wavelength-tunable photoluminescence. *Chemical communications (Cambridge, England)*, (25):3759–61, July 2009. ISSN 1359-7345. doi: 10.1039/b903313k. URL http://www.ncbi.nlm.nih.gov/pubmed/19557273.

[35] Jun-Wei Luo, Paul Stradins, and Alex Zunger. Matrix-embedded silicon quantum dots for photovoltaic applications: a theoretical study of critical factors. *Energy & Environmental Science*, 4(7):2546, 2011. ISSN 1754-5692. doi: 10.1039/c1ee01026c. URL http://xlink.rsc.org/?DOI=c1ee01026c.

[36] K.R. Williams and R.S. Muller. Etch rates for micromachining processing. *Journal of Microelectromechanical Systems*, 5(4):256–269, 1996. ISSN 10577157. doi: 10.1109/84.546406. URL http://ieeexplore.ieee.org/lpdocs/epic03/wrapper.htm?arnumber=546406.

[37] KR Williams, Kishan Gupta, and Matthew Wasilik. Etch rates for micromachining processing-Part II. *Journal of Microelectromechanical Systems*, 12(6):761–778, 2003. URL http://ieeexplore.ieee.org/xpls/abs_all.jsp?arnumber=1257354.

[38] Harry Robbins and Bertram Schwartz. Chemical Etching of Silicon. *Journal of The Electrochemical Society*, 106(6):505, 1959. ISSN 00134651. doi: 10.1149/1.2427397. URL http://jes.ecsdl.org/cgi/doi/10.1149/1.2427397.

[39] H. Robbins and B. Schwartz. Chemical Etching of Silicon. *Journal of The Electrochemical Society*, 107(2):108, 1960. ISSN 00134651. doi: 10.1149/1.2427617. URL http://jes.ecsdl.org/cgi/doi/10.1149/1.2427617.

[40] B. Schwartz and H. Robbins. Chemical Etching of Silicon. *Journal of The Electrochemical Society*, 108(4):365, 1961. ISSN 00134651. doi: 10.1149/1.2428090. URL http://jes.ecsdl.org/cgi/doi/10.1149/1.2428090.

[41] B. Schwartz. Chemical Etching of Silicon. *Journal of The Electrochemical Society*, 123 (12):1903, 1976. ISSN 00134651. doi: 10.1149/1.2132721. URL http://jes.ecsdl.org/cgi/doi/10.1149/1.2132721.

[42] Jo Acker, Anja Rietig, Marco Steinert, and Volker Hoffmann. Mass and Electron Balance for the Oxidation of Silicon During the Wet-Chemical Etching in HF/HNO3 Mixtures. *The Journal of Physical Chemistry C*, 20388(5), 2012. URL http://pubs.acs.org/doi/abs/10.1021/jp305621h.

[43] Environmental Health and Safety Office, University of Chicago. Chemical Safety Fact Sheet: Hydrofluoric Acid. http://www.uic.edu/depts/envh/HSS/Documents/.

[44] Jonghoon Choi, Nam Sun Wang, and Vytas Reipa. Photoassisted tuning of silicon nanocrystal photoluminescence. *Langmuir : the ACS journal of surfaces and colloids*, 23(6):3388–94, March 2007. ISSN 0743-7463. doi: 10.1021/la062906+. URL http://www.ncbi.nlm.nih.gov/pubmed/17295527.

[45] Peter Atkins and Ronald Friedman. *Molecular Quantum Mechanics*. Oxford University Press Inc., New York, 2005.

[46] David M. Carey and Gerald M. Korenowski. Measurement of the Raman spectrum of liquid water. *The Journal of Chemical Physics*, 108(7):2669, 1998. ISSN 00219606. doi: 10.1063/1.475659. URL http://link.aip.org/link/JCPSA6/v108/i7/p2669/s1&Agg=doi.

[47] M Ben-Chorin, B Averboukh, D Kovalev, G Polisski, and F Koch. Influence of Quantum Confinement on the Critical Points of the Band Structure of Si. *Physical review letters*, 77(4):763–766, July 1996. ISSN 1079-7114. URL http://www.ncbi.nlm.nih.gov/pubmed/10062896.

[48] J. Heitmann, F. Muller, M. Zacharias, and U. Gosele. Silicon Nanocrystals: Size Matters. *Advanced Materials*, 17(7):795–803, April 2005. ISSN 0935-9648. doi: 10.1002/adma.200401126. URL http://doi.wiley.com/10.1002/adma.200401126.

[49] D. Kovalev, H. Heckler, G. Polisski, and F. Koch. Optical Properties of Si Nanocrystals. *Physica Status Solidi (B)*, 215(2):871–932, October 1999. ISSN 0370-1972. doi: 10.1002/(SICI)1521-3951(199910)215:2⟨871::AID-PSSB871⟩3.0.CO;2-9. URL http://doi.wiley.com/10.1002/%28SICI%291521-3951%28199910%29215%3A2%3C871%3A%3AAID-PSSB871%3E3.0.CO%3B2-9.

[50] G. Ledoux, J. Gong, F. Huisken, O. Guillois, and C. Reynaud. Photoluminescence of size-separated silicon nanocrystals: Confirmation of quantum confinement. *Applied Physics Letters*, 80(25):4834, 2002. ISSN 00036951. doi: 10.1063/1.1485302. URL http://link.aip.org/link/APPLAB/v80/i25/p4834/s1&Agg=doi.

[51] Douglas S. English, Lindsay E. Pell, Zhonghua Yu, Paul F. Barbara, and Brian A. Korgel. Size Tunable Visible Luminescence from Individual Organic Monolayer Stabilized Silicon Nanocrystal Quantum Dots. *Nano Letters*, 2(7):681–685, July 2002. ISSN 1530-6984. doi: 10.1021/nl025538c. URL http://pubs.acs.org/doi/abs/10.1021/nl025538c.

[52] Daniel C Hannah, Jihua Yang, Paul Podsiadlo, Maria K Y Chan, Arnaud Demortière, David J Gosztola, Vitali B Prakapenka, George C Schatz, Uwe Kortshagen, and Richard D Schaller. On the origin of photoluminescence in silicon nanocrystals: pressure-dependent structural and optical studies. *Nano letters*, 12(8):4200–5, August 2012. ISSN 1530-6992. doi: 10.1021/nl301787g. URL http://www.ncbi.nlm.nih.gov/pubmed/22757779.

[53] Colin M. Hessel, Dariya Reid, Matthew G. Panthani, Michael R. Rasch, Brian W. Goodfellow, Junwei Wei, Hiromasa Fujii, Vahid Akhavan, and Brian a. Korgel. Synthesis of Ligand-Stabilized Silicon Nanocrystals with Size-Dependent Photoluminescence Spanning Visible to Near-Infrared Wavelengths. *Chemistry of Materials*, 24 (2):393–401, January 2012. ISSN 0897-4756. doi: 10.1021/cm2032866. URL http://pubs.acs.org/doi/abs/10.1021/cm2032866.

[54] Amir Saar. Photoluminescence from silicon nanostructures: The mutual role of quantum confinement and surface chemistry. *Journal of Nanophotonics*, 3(1):032501, March 2009. ISSN 1934-2608. doi: 10.1117/1.3111826. URL http://nanophotonics.spiedigitallibrary.org/article.aspx?doi=10.1117/1.3111826.

[55] M. Wolkin, J. Jorne, P. Fauchet, G. Allan, and C. Delerue. Electronic States and Luminescence in Porous Silicon Quantum Dots: The Role of Oxygen. *Physical Review Letters*, 82(1):197–200, January 1999. ISSN 0031-9007. doi: 10.1103/PhysRevLett.82.197. URL http://link.aps.org/doi/10.1103/PhysRevLett.82.197.

[56] Anoop Gupta and Hartmut Wiggers. Freestanding silicon quantum dots: origin of red and blue luminescence. *Nanotechnology*, 22(5):055707, February 2011. ISSN 1361-6528. doi: 10.1088/0957-4484/22/5/055707. URL http://www.ncbi.nlm.nih.gov/pubmed/21178223.

[57] CS Yang and RA Bley. Synthesis of alkyl-terminated silicon nanoclusters by a solution route. *Journal of the ...*, (20):5191–5195, 1999. URL http://pubs.acs.org/doi/abs/10.1021/ja9828509.

[58] S Godefroo, M Hayne, M Jivanescu, a Stesmans, M Zacharias, O I Lebedev, G Van Tendeloo, and V V Moshchalkov. Classification and control of the origin of photoluminescence from Si nanocrystals. *Nature nanotechnology*, 3(3):174–8, March 2008. ISSN 1748-3395. doi: 10.1038/nnano.2008.7. URL http://www.ncbi.nlm.nih.gov/pubmed/18654491.

[59] I. E. Anderson, R. A. Shircliff, C. Macauley, D. K. Smith, B. G. Lee, S. Agarwal, P. Stradins, and R. T. Collins. Silanization of Low-Temperature-Plasma Synthesized Silicon Quantum Dots for Production of a Tunable, Stable, Colloidal Solution. *The Journal of Physical Chemistry C*, 116(6):3979–3987, February 2012. ISSN 1932-7447. doi: 10.1021/jp211569a. URL http://pubs.acs.org/doi/abs/10.1021/jp211569a.

[60] Wolfram Mathematica 8 for Students. By Wolfram Research, Inc. Licensed Software.

[61] C Delerue, G Allan, and M Lannoo. Theoretical aspects of the luminescence of porous silicon. *Physical Review B*, 48(15):24–36, 1993.

[62] P F Trwoga, A J Kenyon, and C W Pitt. Modeling the contribution of quantum confinement to luminescence from silicon nanoclusters. *Journal of Applied Physics*, 83 (7):1–6, 1998.

[63] C. Garoufalis, Aristides Zdetsis, and Stefan Grimme. High Level Ab Initio Calculations of the Optical Gap of Small Silicon Quantum Dots. *Physical Review Letters*, 87(27): 276402, December 2001. ISSN 0031-9007. doi: 10.1103/PhysRevLett.87.276402. URL http://link.aps.org/doi/10.1103/PhysRevLett.87.276402.

[64] B Delley and E F Steigmeier. Quantum confinement in Si nanocrystals. *Physical Review B*, 47(3):1397–1400, 1993.

[65] Xuegeng Li, Yuanqing He, and Mark T Swihart. Surface functionalization of silicon nanoparticles produced by laser-driven pyrolysis of silane followed by HF-HNO3 etching. *Langmuir : the ACS journal of surfaces and colloids*, 20(11):4720–7, May 2004. ISSN 0743-7463. URL http://www.ncbi.nlm.nih.gov/pubmed/15969188.

[66] Fengjun Hua, Mark T Swihart, and Eli Ruckenstein. Efficient surface grafting of luminescent silicon quantum dots by photoinitiated hydrosilylation. *Langmuir : the ACS journal of surfaces and colloids*, 21(13):6054–62, June 2005. ISSN 0743-7463. doi: 10.1021/la0509394. URL http://www.ncbi.nlm.nih.gov/pubmed/15952860.

[67] CM Hessel, EJ Henderson, and JGC Veinot. Hydrogen silsesquioxane: A molecular precursor for nanocrystalline Si-SiO2 composites and freestanding hydride-surface-terminated silicon nanoparticles. *Chemistry of materials*, (1):6139–6146, 2006. doi: 10.1039/b607476f.Bulk. URL http://pubs.acs.org/doi/abs/10.1021/cm0602803.

[68] Joel A Kelly, Amber M Shukaliak, Michael D Fleischauer, and Jonathan G C Veinot. Size-dependent reactivity in hydrosilylation of silicon nanocrystals. *Journal of the American Chemical Society*, 133(24):9564–71, June 2011. ISSN 1520-5126. doi: 10.1021/ja2025189. URL http://www.ncbi.nlm.nih.gov/pubmed/21595468.

[69] A. G. Cullis, L.T. Canham, and P.D.J Calcott. The structural and luminescence properties of porous silicon. *J.Appl.Phys.*, 82(August 1997):909–965, 1997.

[70] Seiichi Sato, Takatoshi Ikeda, Kengo Hamada, and Keisaku Kimura. Size regulation by bandgap-controlled etching: Application to germanium nanoparticles. *Solid State Communications*, 149(21-22):862–865, June 2009. ISSN 00381098. doi: 10.1016/j.ssc.2009.03.008. URL http://linkinghub.elsevier.com/retrieve/pii/S0038109809001306.

[71] Ruben Oren and Sorab K. Ghandhi. Ultraviolet-Enhanced Oxidation of Silicon. *Journal of Applied Physics*, 42(2):752, 1971. ISSN 00218979. doi: 10.1063/1.1660091. URL http://link.aip.org/link/?JAP/42/752/1&Agg=doi.

[72] E. M. Young. Electron-active silicon oxidation. *Applied Physics A Solids and Surfaces*, 47(3):259–269, November 1988. ISSN 0721-7250. doi: 10.1007/BF00615932. URL http://link.springer.com/10.1007/BF00615932.

[73] Jose R. Rodríguez Núñez, Joel a. Kelly, Eric J. Henderson, and Jonathan G. C. Veinot. Wavelength-Controlled Etching of Silicon Nanocrystals. *Chemistry of Materials*, 24 (2):346–352, January 2012. ISSN 0897-4756. doi: 10.1021/cm203085f. URL http://pubs.acs.org/doi/abs/10.1021/cm203085f.

[74] E Yablonovitch, D.L Allara, C.C Chang, T Gmitter, and T.B Bright. Unusually low surface-recombination velocity on silicon and germanium surfaces. *Physical Review Letters*, 57(2), 1986.

[75] H Bender, S Verhaverbeke, and M.M Heyns. Hydrogen Passivation of HF-Last Cleaned (100) Silicon Surfaces Investigated by Multiple Internal Reflection Infrared Spectroscopy. *Solid State Science and Technology*, 141(11), 1994.

[76] Sanjukta Guhathakurta and Anuradha Subramanian. Effect of Hydrofluoric Acid in Oxidizing Acid Mixtures on the Hydroxylation of Silicon Surface. pages 136–146, 2007. doi: 10.1149/1.2779951.

[77] Anoop Gupta, Ahmed S G Khalil, Markus Winterer, and Hartmut Wiggers. Stable Colloidal Dispersions of Silicon Nanoparticles for the Fabrication of Films using Inkjet Printing Technology. *3rd IEEE International Nanoelectronics Conference*, 1-2:0–1, 2010.

[78] R. Lockwood, S. McFarlane, J.R. Rodríguez Núñez, X.Y. Wang, J.G.C. Veinot, and a. Meldrum. Photoactivation of silicon quantum dots. *Journal of Luminescence*, 131 (7):1530–1535, July 2011. ISSN 00222313. doi: 10.1016/j.jlumin.2011.02.006. URL `http://linkinghub.elsevier.com/retrieve/pii/S0022231311000391`.

[79] R. T. Collins, M. A. Tischler, and J. H. Stathis. Photoinduced hydrogen loss from porous silicon. *Applied Physics Letters*, 61(14):1649, 1992. ISSN 00036951. doi: 10.1063/1.108440. URL `http://link.aip.org/link/APPLAB/v61/i14/p1649/s1&Agg=doi`.

[80] M. A. Tischler, R. T. Collins, J. H. Stathis, and J. C. Tsang. Luminescence degradation in porous silicon. *Applied Physics Letters*, 60(5):639, 1992. ISSN 00036951. doi: 10.1063/1.106578. URL `http://link.aip.org/link/APPLAB/v60/i5/p639/s1&Agg=doi`.

[81] Stephen G. Boyes. Professor in the Department of Chemistry and Geochemistry at Colorado School of Mines, Personal communication, March 21st, 2013.

[82] B Garrido, M Lopez, a Perezrodriguez, C Garcia, P Pellegrino, R Ferre, J Moreno, J Morante, C Bonafos, and M Carrada. Optical and electrical properties of Si-nanocrystals ion beam synthesized in SiO2. *Nuclear Instruments and Methods in Physics Research Section B: Beam Interactions with Materials and Atoms*, 216:213–221, February 2004. ISSN 0168583X. doi: 10.1016/j.nimb.2003.11.037. URL `http://linkinghub.elsevier.com/retrieve/pii/S0168583X03021499`.

[83] J. S. Biteen, N. S. Lewis, H. A. Atwater, and A. Polman. Size-dependent oxygen-related electronic states in silicon nanocrystals. *Applied Physics Letters*, 84(26):5389, 2004. ISSN 00036951. doi: 10.1063/1.1765200. URL `http://link.aip.org/link/APPLAB/v84/i26/p5389/s1&Agg=doi`.

[84] Jörg Martin, Frank Cichos, Friedrich Huisken, and Christian von Borczyskowski. Electron-phonon coupling and localization of excitons in single silicon nanocrystals. *Nano letters*, 8(2):656–60, February 2008. ISSN 1530-6984. doi: 10.1021/nl0731163. URL `http://www.ncbi.nlm.nih.gov/pubmed/18197721`.

[85] Fulin Zhou and John D Head. Role of SidO in the Photoluminescence of Porous Silicon. *J.Phys.Chem. B*, 104:9981–9986, 2000.

[86] A Kux and M Ben-Chorin. Band gap of porous silicon. *Physical Review B*, 51(24):17535–17541, 1995.

[87] Joseph B Miller, Austin R Van Sickle, Rebecca J Anthony, Daniel M Kroll, Uwe R Kortshagen, and Erik K Hobbie. Ensemble brightening and enhanced quantum yield in size-purified silicon nanocrystals. *ACS nano*, 6(8):7389–96, August 2012. ISSN 1936-086X. doi: 10.1021/nn302524k. URL http://www.ncbi.nlm.nih.gov/pubmed/22809465.

[88] Ingrid E. Anderson. Postdoctoral Fellow in the Department of Physics at Colorado School of Mines, Personal communication, March 14th, 2013.

[89] D Kovalev, J Diener, H Heckler, G Polisski, N Kunzner, and F Koch. Optical absorption cross sections of Si nanocrystals. *Physical Review B*, 61(7):4485–4487, 2000. URL http://prb.aps.org/abstract/PRB/v61/i7/p4485_1.

[90] Joel A Kelly and Jonathan G C Veinot. An investigation into near-UV hydrosilylation of freestanding silicon nanocrystals. *ACS Nano*, 4(8):4645–56, August 2010. ISSN 1936-086X. doi: 10.1021/nn101022b. URL http://www.ncbi.nlm.nih.gov/pubmed/20731446.

[91] Seiichi Sato and Mark T. Swihart. Propionic-Acid-Terminated Silicon Nanoparticles: Synthesis and Optical Characterization. *Chemistry of Materials*, 18(17):4083–4088, August 2006. ISSN 0897-4756. doi: 10.1021/cm060750t. URL http://pubs.acs.org/doi/abs/10.1021/cm060750t.

[92] J D Holmes, K J Ziegler, R C Doty, L E Pell, K P Johnston, and B A Korgel. Highly luminescent silicon nanocrystals with discrete optical transitions. *Journal of the American Chemical Society*, 123(16):3743–8, April 2001. ISSN 0002-7863. URL http://www.ncbi.nlm.nih.gov/pubmed/11457106.

[93] LE Brus, PF Szajowski, WL Wilson, TD Harris, S Schuppler, and PH Citrin. Electronic spectroscopy and photophysics of Si nanocrystals: relationship to bulk c-Si and porous Si. *Journal of the American Chemical Society*, 117(10):2915–2922, 1995. URL http://pubs.acs.org/doi/abs/10.1021/ja00115a025.

[94] J. Wilcoxon, G. Samara, and P. Provencio. Optical and electronic properties of Si nanoclusters synthesized in inverse micelles. *Physical Review B*, 60(4):2704–2714, July 1999. ISSN 0163-1829. doi: 10.1103/PhysRevB.60.2704. URL http://link.aps.org/doi/10.1103/PhysRevB.60.2704.

[95] Jamie H Warner, Akiyoshi Hoshino, Kenji Yamamoto, and Richard D Tilley. Water-soluble photoluminescent silicon quantum dots. *Angewandte Chemie (International ed. in English)*, 44(29):4550–4, July 2005. ISSN 1433-7851. doi: 10.1002/anie.200501256. URL http://www.ncbi.nlm.nih.gov/pubmed/15973756.

[96] M. V. Rama Krishna and R. A. Friesner. Prediction of anomalous redshift in semiconductor clusters. *The Journal of Chemical Physics*, 96(2):873, 1992. ISSN 00219606. doi: 10.1063/1.462158. URL http://link.aip.org/link/JCPSA6/v96/i2/p873/s1&Agg=doi.

[97] Y. Ma and J. A. Eades. Analyses of HF/NH4F buffer-treated Si(111) surfaces using XPS, REM and SIMS. *Applied Physics A Materials Science & Processing*, 62(3):247–253, March 1996. ISSN 0947-8396. doi: 10.1007/BF01575089. URL http://link.springer.com/10.1007/BF01575089.

[98] David Jurbergs, Elena Rogojina, Lorenzo Mangolini, and Uwe Kortshagen. Silicon nanocrystals with ensemble quantum yields exceeding 60%. *Applied Physics Letters*, 88 (23):233116, 2006. ISSN 00036951. doi: 10.1063/1.2210788. URL http://link.aip.org/link/APPLAB/v88/i23/p233116/s1&Agg=doi.

[99] Melanie L Mastronardi, Florian Maier-Flaig, Daniel Faulkner, Eric J Henderson, Christian Kübel, Uli Lemmer, and Geoffrey A Ozin. Size-dependent absolute quantum yields for size-separated colloidally-stable silicon nanocrystals. *Nano letters*, 12 (1):337–42, January 2012. ISSN 1530-6992. doi: 10.1021/nl2036194. URL http://www.ncbi.nlm.nih.gov/pubmed/22195549.

APPENDIX - SPECIFICATIONS OF EXPERIMENTAL SETUPS

A.1 PL- and PLE-system

The mercury-arc lamp used as an excitation source was a 100W Apex Arc lamp from Newport, model number 66456. The 365 nm line was picked out by two bandpass filters from Edmund Optics, part number 65130, mounted in series in a Newport lens holder, model number 6195. This setup prevented any appreciable leakage from any of the other mercury lines. The stability of the lamp output intensity was measured to vary less than 5 % over the course of 5 hours, and less than 3 % within any 10 minute interval. PL emission was dispersed with an Acton SP 300i spectrometer, using a grating with 150 gr/mm, blazed at 800 nm. The signal was recorded by a Spec-10:100BR LN cooled c-Si CCD-array. Both spectrometer and CCD-array were from Princeton Instruments/Roper Scientific. Software used to operate the system was WinSpec version 2.5.23.0 from Roper Scientific.

For PLE, a NanoLog system from Horiba Jobin Yvon was used, model number FL-1000. The excitation source was a 450 W xenon lamp from the same company, model number FL-1039/40. The excitation wavelength was picked out by a spectrometer using a grating with 1200 gr/mm, blazed at 330 nm. The grating in front of the emission detector has a density of 1200 gr/mm, blazed at 500 nm. The detector was a photomultiplier tube (PMT).

Excitation power was measured by a FieldMax II TO powermeter with a OP-2 UV detector head, both from Coherent.

A.1.1 Correction for spectral response

The spectral response correction curve for the PL-detection system, with the grating centered at 650 nm is shown in Figure A.1. This curve was obtained by measuring a 20 Watt Quartz Tungsten Halogen bulb from Oriel, model number 6319, with no filters in front of the detection system. This bulb has a known, smooth spectral curve ranging from near-UV into the visible. The normalized spectrum of the lamp was divided by the normalized

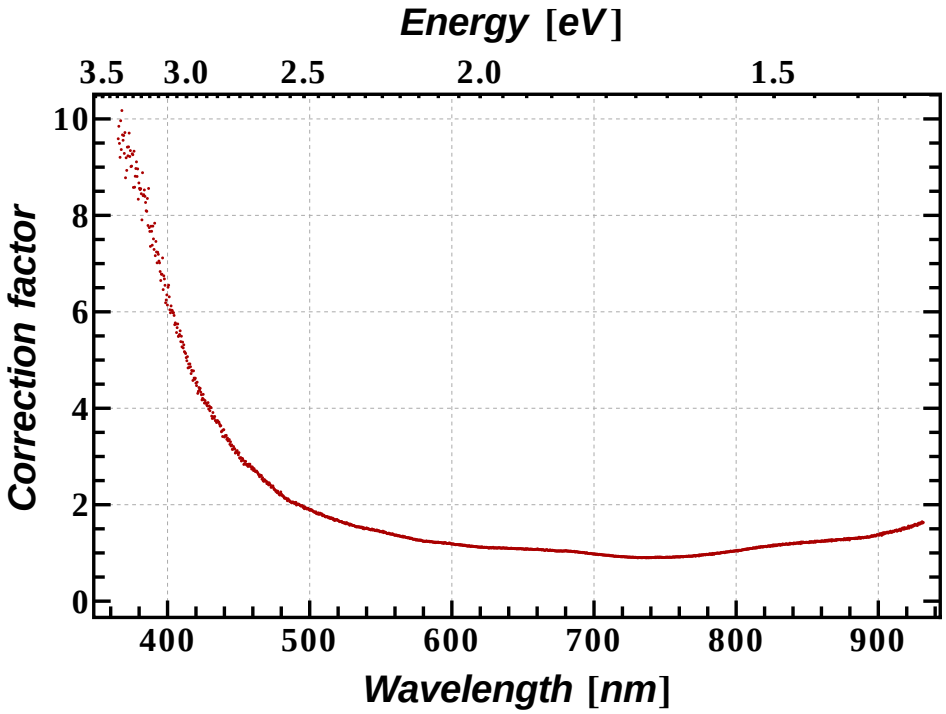

Figure A.1: Spectral response curve for PL detection system

output of the system, yielding the correction curve shown. For all spectra, the value at any given wavelength was corrected for spectral response by multiplying with the corresponding correction factor from this curve.

For PL measurements in the NanoLog system, PL spectra were also acquired to determine the emission detection wavelength for PLE, as described in 2.5.1. In addition to the detector measuring emission, which was corrected for spectral response, the PLE spectra were corrected for changes in lamp intensity in the Xenon lamp used for excitation. This was measured by another detector with its own spectral response. The correction files for these two detectors came from the manufacturer, and are plotted in Figure A.2.

A.2 Chemicals

Etchant was mixed to desired concentrations from 48 % HF purchased from Macron Chemicals and 68 % HNO_3 purchased from Malinckrodt Chemicals. High purity deionized water (18.5 MΩ/cm) was obtained from an Aqua Solution water purification system. Ethanol

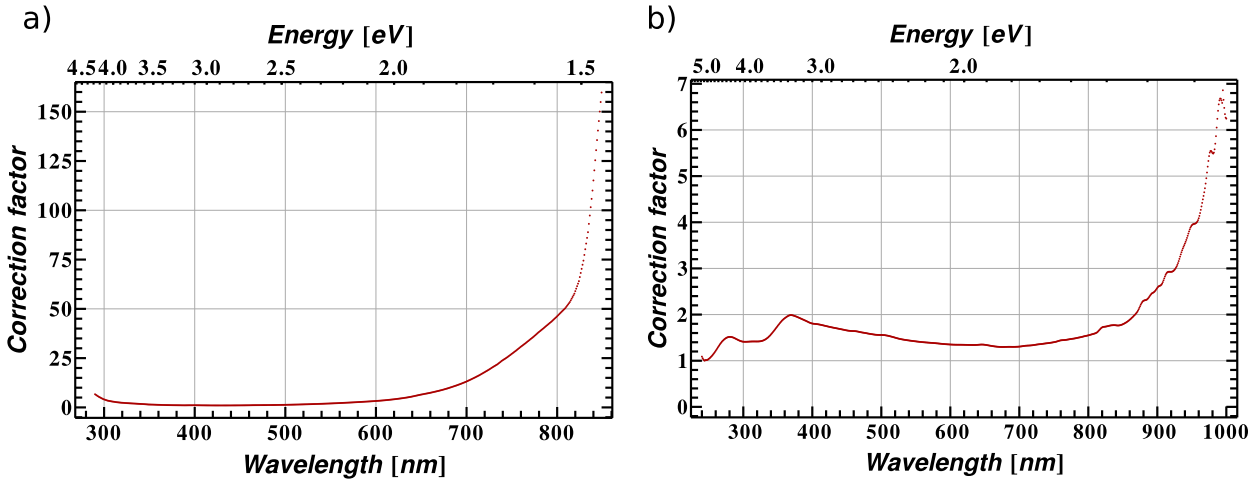

Figure A.2: Spectral response curve for fluorolog used for PL/PLE. a) Spectral response emission detector. b) Spectral response excitation intensity detector.

used was 200 proof- Absolute reagent grade ethanol, purchased from Pharmco-Aaper.

A.3 Scale

The scale used for all weighing was a Sartorius CPA 225 D. It was last calibrated by Data Weighing Systems on 05.15.12.

A.4 TEM

All TEM-work was done with a FEI Company CM200 microscope with a LaB_6 filament and a 200 kV accelerating voltage. Samples were prepared on a holey carbon copper coated grid.